

Complexity Transitions in Non-Unitary Boson Sampling Dynamics

Ken Mochizuki¹ and Ryusuke Hamazaki^{1,2}

¹*Nonequilibrium Quantum Statistical Mechanics RIKEN Hakubi Research Team,
RIKEN Cluster for Pioneering Research (CPR), 2-1 Hirosawa, Wako 351-0198, Japan*

²*RIKEN Interdisciplinary Theoretical and Mathematical Sciences Program (iTHEMS), 2-1 Hirosawa, Wako 351-0198, Japan*

We discover novel transitions characterized by computational complexity in non-unitary dynamics of bosons with parity-time (\mathcal{PT}) symmetry. We show that parity-time (\mathcal{PT}) symmetry breaking, a unique transition in non-Hermitian systems, profoundly affects the complexity of sampling the probability distribution of bosons. In a \mathcal{PT} -symmetric phase, we find only one dynamical transition, upon which the distribution of bosons ceases to be approximated by a computable one for distinguishable particles. If the system enters a \mathcal{PT} -broken phase, the threshold time for the transition is suddenly prolonged. Furthermore, this phase also exhibits a notable dynamical transition on a longer time scale, at which the boson distribution again becomes computable. This transition, and hence the easiness of the boson sampling problem in long times, are true for generic postselected non-unitary quantum dynamics.

Introduction.— The last decade has witnessed a rapid progress of our understanding in non-Hermitian quantum mechanics, which provides an effective description of open quantum systems that exhibit non-unitary dynamics. Indeed, various intriguing phenomena have been revealed, such as effects of disorder [1–12], parity-time (\mathcal{PT}) symmetry breaking [13–37], and topological phenomena [30, 36, 38–61]. Interestingly, non-Hermitian dynamics has been observed not only in genuinely quantum systems, such as photonic systems [30, 58, 62] and ultracold atomic systems [33, 37], but also in classical systems [19, 20, 24–27, 40, 55]. In that sense, it is a fundamental but largely unexplored question to what extent non-Hermitian quantum mechanics exhibits unique quantum nature distinct from classical systems.

In unitary quantum dynamics, unique quantum nature can be discussed by its computational complexity, which is investigated in the boson sampling problem [63–88]. In this problem, probability distributions of photons in optical networks can be hard to sample by classical computers, which suggests the quantum supremacy [64]. Recent study suggests that the computational complexity can be used to diagnose various phases and states of photons [71, 81] since each physical situation determines whether or not the boson sampling problem is hard.

In this Letter, we report novel transitions concerning the computational complexity of many-photon probability distributions in non-unitary quantum dynamics. We find that \mathcal{PT} -symmetry breaking, a unique phenomenon due to non-unitarity [13–37], enhances the regime for which the boson sampling is classically easy. In a \mathcal{PT} -symmetric phase, there is a single dynamical transition as in isolated systems [81], where the actual distribution ceases to be approximated by a classically computable one for distinguishable particles. Upon \mathcal{PT} -symmetry breaking, the corresponding transition time is suddenly prolonged. Remarkably, we discover an additional dynamical transition in the later stage where the distribution is

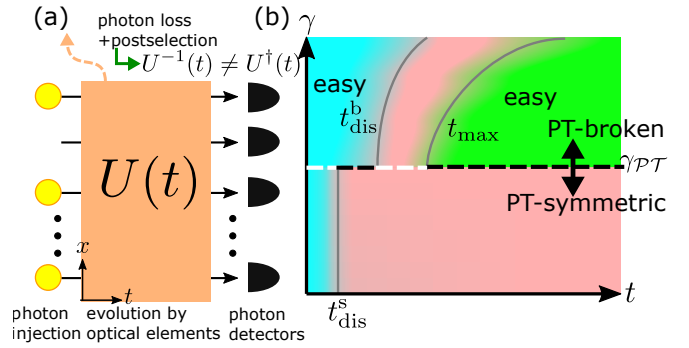


FIG. 1. (a) Schematic picture for the non-unitary boson sampling. Photons experience non-unitary dynamics by $U(t) (\neq [U^\dagger(t)]^{-1})$ through linear optical elements with loss effects, where we postselect cases for which all photons remain in the system. (b) Schematic phase diagram for the complexity to sample photon distributions. Times t_{dis}^s and t_{dis}^b with $t_{\text{dis}}^s \ll t_{\text{dis}}^b$ are thresholds for the short-time dynamical complexity transition in \mathcal{PT} -symmetric and \mathcal{PT} -broken phases, respectively. Time t_{max} is a threshold time for the long-time transition in the \mathcal{PT} -broken phase. In blue and green regions, the distribution is sampled efficiently, where the latter is unique to non-unitary dynamics. We conjecture that a classically hard regime exists in the red region.

essentially determined by the dominant eigenmode of the non-unitary operator, which makes it classically computable again. We also show that this long-time transition is generic for postselected non-unitary dynamics.

Model and \mathcal{PT} symmetry breaking.— To consider the non-unitary boson sampling problem for dynamics with \mathcal{PT} -symmetry illustrated in Fig. 1 (a), we first introduce a model of discrete-time quantum walks, which are versatile platforms for exploring quantum statistics [89–96] and non-unitary dynamics [28, 30, 34–36, 58, 97]. There, photons with two internal polarization states propagate through an optical network with L sites, as

detailed in Supplemental Material [98]. In our one-dimensional system, the single-photon evolution operator for each timestep, parametrized by the rotation angles θ_1, θ_2 and gain/loss strength γ , reads

$$V = C(\theta_1/2)SG(\gamma)C(\theta_2)G(-\gamma)SC(\theta_1/2), \quad (1)$$

where

$$C(\theta) = I_x \otimes e^{-i\theta\sigma_2}, \quad G(\gamma) = I_x \otimes e^{\gamma\sigma_3},$$

$$S = \sum_{x=1}^L \begin{pmatrix} |x-1\rangle\langle x| & 0 \\ 0 & |x+1\rangle\langle x| \end{pmatrix} = \sum_k |k\rangle\langle k| \otimes e^{ik\sigma_3}. \quad (2)$$

Here, the basis set is represented as $\hat{b}_{x,h}^\dagger |0\rangle = |x, h\rangle = |x\rangle \otimes (1, 0)^T$ and $\hat{b}_{x,v}^\dagger |0\rangle = |x, v\rangle = |x\rangle \otimes (0, 1)^T$, where $x \in [1, 2, \dots, L]$ is the position with the periodic boundary condition, $\sigma = h/v$ denotes the horizontal/vertical polarization, $\hat{b}_{x,\sigma}^\dagger$ is a creation operator of a photon at x with σ , and $|0\rangle$ is the vacuum. In addition, $\sigma_{1,2,3}$ are the Pauli matrices acting on the polarization, $I_x = \sum_{x=1}^L |x\rangle\langle x|$, and the Fourier transform has been made for S with a momentum basis $|k\rangle$. Single-photon dynamics for one timestep satisfies $|\psi(t+1)\rangle = V|\psi(t)\rangle / \sqrt{\langle\psi(t)|V^\dagger V|\psi(t)\rangle}$.

The time-evolution operator respects \mathcal{PT} symmetry $(\mathcal{PT})V(\mathcal{PT})^{-1} = V^{-1}$ with $\mathcal{PT} = \sum_x |-x\rangle\langle x| \otimes \sigma_3 \mathcal{K}$, where \mathcal{K} is the complex-conjugation operator. Introducing the momentum-space representation of V , i.e., $V = \sum_k |k\rangle\langle k| \otimes \tilde{V}(k)$ [28, 36] with $\tilde{V}(k) = e^{-i\theta_1\sigma_2/2} e^{(\gamma+ik)\sigma_3} e^{-i\theta_2\sigma_2} e^{(ik-\gamma)\sigma_3} e^{-i\theta_1\sigma_2/2}$, the symmetry can equivalently be written as $\sigma_3 \tilde{V}^*(k) \sigma_3 = \tilde{V}^{-1}(k)$. Solving the eigen-equation $\tilde{V}(k) |\phi_\pm^R(k)\rangle = \lambda_\pm(k) |\phi_\pm^R(k)\rangle$, we can derive $\lambda_\pm(k) = e^{-i\varepsilon_\pm(k)} = d(k) \pm \sqrt{d^2(k) - 1}$, where $\varepsilon_\pm(k)$ is the quasi-energy and $d(k) = \cos(\theta_1) \cos(\theta_2) \cos(2k) - \sin(\theta_1) \sin(\theta_2) \cosh(2\gamma)$. In a \mathcal{PT} -symmetric phase, $\sigma_3 \mathcal{K} |\phi_\pm^R(k)\rangle = |\phi_\pm^R(k)\rangle$ and $|\lambda_\pm(k)| = 1$ for all k . In a \mathcal{PT} -broken phase, however, $\sigma_3 \mathcal{K} |\phi_\pm^R(k)\rangle \neq |\phi_\pm^R(k)\rangle$ and $|\lambda_\pm(k)| \neq 1$ for some k . Increasing the gain-loss parameter γ with θ_1, θ_2 being fixed, the present model exhibits the transition from the \mathcal{PT} -symmetric phase to the \mathcal{PT} -broken phase.

Non-unitary boson sampling problem.- In the boson sampling problem, we consider linear dynamics where input M -mode bosons are transformed by an M -by- M matrix $U(t)$, as schematically described in Fig. 1 (a). While previous works focus on unitary $U(t)$, we here consider the non-unitary \mathcal{PT} -symmetric Floquet model introduced above and set $U^T(t) = V^t$, where T is the transpose. The basis of $U(t)$ is labeled by the positions and polarizations of a photon with an index $j = (x, \sigma)$ and thus $M = 2L$. We can characterize the input state in two ways. One way is to label the state by the index $j = (x, \sigma)$ for each photon: the state is given by $\{\ln\} = (\ln_1, \dots, \ln_n)$, where $\ln_p = (x_p^{\text{in}}, \sigma_p^{\text{in}})$ is the corresponding index for the p th input photon, and n

is the total number of photons. The other way is to characterize the input state by the number of photons at each j , i.e., $\{n^{\text{in}}\} = (n_1^{\text{in}}, \dots, n_M^{\text{in}})$ with $\sum_j n_j^{\text{in}} = n$. As shown in Supplemental Material [98], a normalized state $\prod_{p=1}^n \hat{b}_{\ln_p}^\dagger |0\rangle / \prod_{j=1}^M \sqrt{n_j^{\text{in}}!}$ is transformed as

$$\frac{\prod_{p=1}^n \hat{b}_{\ln_p}^\dagger |0\rangle}{\prod_{j=1}^M \sqrt{n_j^{\text{in}}!}} \rightarrow \frac{\prod_{p=1}^n \left[\sum_{j=1}^M U_{\ln_p j}(t) \hat{b}_j^\dagger \right] |0\rangle}{\sqrt{N(t)} \prod_{j=1}^M \sqrt{n_j^{\text{in}}!}}, \quad (3)$$

where $N(t)$ is a normalization factor, which is unity only when $U(t)$ is unitary. For our case, $U(t)$ is non-unitary unless $e^\gamma = 1$.

From Eq. (3), the output probability distribution of photons, characterized by $\{n^{\text{out}}\} = (n_1^{\text{out}}, \dots, n_M^{\text{out}})$ with $\sum_j n_j^{\text{out}} = n$, becomes

$$P(\{n^{\text{in}}\}, \{n^{\text{out}}\}, t) = \frac{|\text{Per}[W(t)]|^2}{N(t) \prod_{j=1}^M n_j^{\text{in}}! n_j^{\text{out}}!}. \quad (4)$$

Here, $\text{Per}[W(t)]$ is the permanent of n -by- n matrix $W(t)$ defined as $W_{pq}(t) = U_{\text{In}_p \text{Out}_q}(t)$, where $\text{Out}_q = (x_q^{\text{out}}, \sigma_q^{\text{out}})$ is the label for the q th output photon. Note that Eq. (4) has the same form with the unitary case [99] except for the normalization factor $N(t)$.

The essence of the boson sampling problem is that $P(\{n^{\text{in}}\}, \{n^{\text{out}}\}, t)$ can be hard to sample by a classical computer. For example, Ref. [64] provided a plausible conjecture based on a polynomial hierarchy that the problem is $\#P$ -hard when $U(t)$ is a Gaussian random unitary matrix. On the other hand, constraints on $U(t)$, such as the positivity of matrix elements or the generatability by short-time dynamics of local Hamiltonians, result in distributions that are efficiently sampled [63, 81]. To explore whether or not sampling $P(\{n^{\text{in}}\}, \{n^{\text{out}}\}, t)$ is efficiently carried out, we evaluate the L_1 -distance between $P(\{n^{\text{in}}\}, \{n^{\text{out}}\}, t)$ and another reference distribution $Q(\{n^{\text{in}}\}, \{n^{\text{out}}\}, t)$,

$$|P(t) - Q(t)| = \sum_{\{n^{\text{out}}\}} |P(\{n^{\text{out}}\}, t) - Q(\{n^{\text{out}}\}, t)|. \quad (5)$$

Here, $\{n^{\text{in}}\}$ is omitted for brevity throughout the manuscript, if there is no confusion. If sampling $Q(\{n^{\text{out}}\}, t)$ is classically efficient and $|P(t) - Q(t)| < \delta$ is satisfied with a small constant δ , sampling $P(\{n^{\text{out}}\}, t)$ is classically easy within the precision δ [81].

Complexity transition in the short-time regime.- Let us first discuss the short-time dynamical complexity transition. If we place the input photons well separated from one another with the distance L/n , they are approximately regarded as distinguishable particles for early times. Then, $P(\{n^{\text{in}}\}, \{n^{\text{out}}\}, t)$ is approximated by a distribution for distinguishable particles given by

$$P_{\text{dis}}(\{n^{\text{in}}\}, \{n^{\text{out}}\}, t) = \frac{\sum_{\omega} \prod_{p=1}^n |U_{\ln_p \text{Out}_{\omega(p)}}(t)|^2}{N_{\text{dis}}(t) \prod_{j=1}^M n_j^{\text{in}}! n_j^{\text{out}}!}. \quad (6)$$

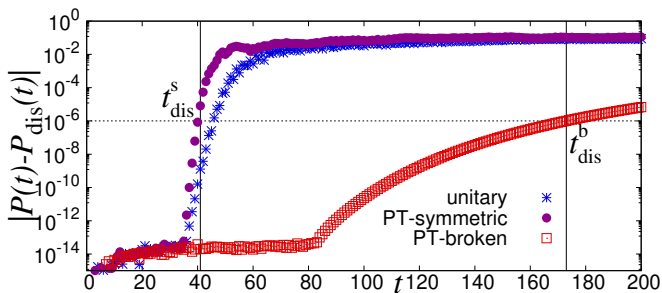


FIG. 2. L_1 -distance between the actual probability distribution of photons $P(\{n^{\text{in}}\}, \{n^{\text{out}}\}, t)$ in Eq. (4) and that for distinguishable particles $P_{\text{dis}}(\{n^{\text{in}}\}, \{n^{\text{out}}\}, t)$ in Eq. (6). After the threshold time $t_{\text{dis}}^{s/b}$, the two distributions differ as $|P(t) - P_{\text{dis}}(t)| > \delta (= 10^{-6})$, which defines the short-time complexity transition. We find that t_{dis}^b for the \mathcal{PT} -broken phase is much larger than t_{dis}^s for the \mathcal{PT} -symmetric phase. The blue asterisks, purple circles, and red squares respectively correspond to $e^\gamma = 1, 1.2$, and 1.5 . The lowest value around 10^{-14} is a numerical artifact. The number of photons is $n = 3$, and the initial state is $\hat{b}_{L/6, h}^\dagger \hat{b}_{L/2, v}^\dagger \hat{b}_{5L/6, v}^\dagger |0\rangle$ with $L = 300$. The rotation angles are $\theta_1 = 0.65\pi$ and $\theta_2 = 0.25\pi$, for which the threshold gain-loss parameter $\gamma_{\mathcal{PT}}$ for \mathcal{PT} symmetry breaking becomes $e^{\gamma_{\mathcal{PT}}} \simeq 1.22$.

Here, ω in the sum is taken over all permutations for the output state, and $N_{\text{dis}}(t)$ is the normalization factor. Sampling $P_{\text{dis}}(\{n^{\text{in}}\}, \{n^{\text{out}}\}, t)$ can be carried out efficiently by classical computers through sampling single-photon distributions [81].

Due to time evolution, photons start to interfere and are no longer approximated by distinguishable particles. Then, a dynamical complexity transition occurs from a phase where $P(\{n^{\text{out}}\}, t)$ is classically easy to sample approximately through $P_{\text{dis}}(\{n^{\text{out}}\}, t)$ to a phase where the method using $P_{\text{dis}}(\{n^{\text{out}}\}, t)$ is impossible. The former and latter phases correspond to the blue and red regions in Fig. 1 (b), respectively. The order parameter for the transition is given by $|P(t) - P_{\text{dis}}(t)|$.

Figure 2 shows numerically obtained L_1 -norm $|P(t) - P_{\text{dis}}(t)|$ with $n = 3$ and the initial distance between photons being $L/n = 100$. We actually find the transition explained above for both \mathcal{PT} -symmetric and \mathcal{PT} -broken phases. The threshold times denoted by t_{dis}^s and t_{dis}^b for these phases are defined as $t_{\text{dis}}^{s/b} = \min t$ s.t. $|P(t) - P_{\text{dis}}(t)| > \delta$ for small $\delta > 0$, which describes the precision of the approximation.

Surprisingly, from Fig. 2, we discover that the threshold time t_{dis}^b is much larger than t_{dis}^s . To understand the prolongation of the threshold time upon \mathcal{PT} breaking, let us evaluate the time scale for the initially separated photons to start to interfere using single-photon dynamics of non-unitary quantum walks. In the \mathcal{PT} -symmetric phase, we find that the quantum walk exhibits the ballistic behavior, which means that the

standard deviation of x behaves as $\sqrt{\langle x^2(t) \rangle - \langle x(t) \rangle^2} \propto t$, where $\langle x^m(t) \rangle = \sum_{x, \sigma} x^m |\psi(x, \sigma, t)|^2$ with $|\psi(t)\rangle = \sum_{x, \sigma} \psi(x, \sigma, t) |x, \sigma\rangle$ [98]. This ballistic dynamics leads to $t_{\text{dis}}^s \propto L/n$. This behavior is similar to that found in unitary dynamics [81]. We note that t_{dis}^s is almost independent of γ .

On the other hand, in the \mathcal{PT} -broken phase, we can show that the single-photon probability distribution becomes asymptotically Gaussian, and the standard deviation of x behaves diffusive as

$$\sqrt{\langle x^2(t) \rangle - \langle x(t) \rangle^2} = \sqrt{\frac{Dt}{2}}, \quad (7)$$

where the diffusion constant is $D = \left| \frac{d^2}{dk^2} \varepsilon_-(k) \right|_{k=0} = |4 \cos(\theta_1) \cos(\theta_2) / \sqrt{d^2(k=0) - 1}|$. In this case, t_{dis}^b is proportional to $(L/n)^2$, which results in $t_{\text{dis}}^b \gg t_{\text{dis}}^s$ for large L . Indeed, as shown in Supplemental Material [98], we can evaluate t_{dis}^b as

$$t_{\text{dis}}^b > \frac{L^2}{2n^2 D |\log(\delta/8n)|}. \quad (8)$$

Since $1/D \propto e^{2\gamma}$ for large γ , t_{dis}^b exhibits an exponential growth as a function of γ , as schematically described in Fig. 1 (b).

For the derivation of the above results, we only use the Fourier analysis and typical dispersion relations in \mathcal{PT} symmetric systems. Therefore, the ballistic-diffusive transition due to \mathcal{PT} -symmetry breaking and the resulting prolongation of the threshold time for the dynamical complexity transition exist in a wide range of \mathcal{PT} -symmetric systems with translation invariance.

Complexity transition in the long-time regime.— Let us next focus on the long-time regime, where we discover a novel dynamical complexity transition at which the problem becomes easy again, unlike unitary dynamics. To this end, we carry out the spectral decomposition of V^t . In the \mathcal{PT} -broken phase, only one eigenstate becomes dominant in the long run, and thus the non-unitary matrix $U^T(t) = V^t$ can be written as

$$U^T(t) \simeq \lambda_{\text{max}}^t |\phi_{\text{max}}^R\rangle \langle \phi_{\text{max}}^L|, \quad (9)$$

where $|\phi_{\text{max}}^R\rangle$ and $|\phi_{\text{max}}^L\rangle$ are respectively right and left eigenstates of V for the largest eigenvalue $|\lambda_{\text{max}}| = \max_{s, k} |\lambda_s(k)| = |\lambda_-(k=0)|$. On the basis of Eq. (9), the permanent of $W(t)$ becomes

$$\text{Per}[W^*(t)] \simeq \lambda_{\text{max}}^{nt} n! \prod_{p=1}^n \langle \text{Out}_p | \phi_{\text{max}}^R \rangle \langle \phi_{\text{max}}^L | \text{In}_p \rangle. \quad (10)$$

The normalization factor is obtained through Eq. (4) and $\sum_{\{n^{\text{out}}\}} P(\{n^{\text{in}}\}, \{n^{\text{out}}\}, t) = 1$, and thus the probability distribution for large t approaches

$$P_{\text{max}}(\{n^{\text{out}}\}) = \frac{\prod_{p=1}^n |\langle \text{Out}_p | \phi_{\text{max}}^R \rangle|^2}{N_{\text{max}} \prod_{j=1}^M n_j^{\text{out}}!}, \quad (11)$$

where $N_{\max} = \langle \phi_{\max}^R | \phi_{\max}^R \rangle^n / n!$. We can show that $P_{\text{dis}}(\{n^{\text{in}}\}, \{n^{\text{out}}\}, t)$ and $P_{\max}(\{n^{\text{out}}\})$ become the same if $U^T(t)$ is written as Eq. (9), which indicates that $P_{\max}(\{n^{\text{out}}\})$ is easy to sample.

After a sufficiently long time, a dynamical complexity transition occurs to a phase where sampling $P(\{n^{\text{out}}\}, t)$ is classically easy approximately through $P_{\max}(\{n^{\text{out}}\})$ from a phase where the approximation to $P_{\max}(\{n^{\text{out}}\})$ is impossible, which respectively correspond to the green and red regions in Fig. 1 (b). The order parameter for the transition is given by $|P(t) - P_{\max}|$.

Figure 3 shows that $|P(t) - P_{\max}|$ actually converges to zero for large t in the \mathcal{PT} -broken phase after the threshold time defined as $t_{\max} = \min t$ s.t. $|P(t) - P_{\max}| < \delta$. The broken lines in Fig. 3 show $e^{-\Delta t}$, where a gap $\Delta = D(2\pi/L)^2/2$ is defined as the difference between the largest value and the second largest value of $\text{Im}[\varepsilon_-(k)]$. From this, we find that the relaxation is governed by Δ . Indeed, we can evaluate the transition time as

$$t_{\max} < \frac{|\log(\delta/8n)|}{\Delta} = \frac{|\log(\delta/8n)|}{2D\pi^2} L^2, \quad (12)$$

which means that the problem inevitably becomes easy for $t > |\log(\delta/8n)|L^2/2D\pi^2$ [98]. We argue that $\log(t_{\max})$ is proportional to γ , as schematically described in Fig. 1 (b), since $1/D \propto e^{2\gamma}$ if γ is large. The inset of Fig. 3 shows that $|P(t) - P_{\text{dis}}(t)|$ also approaches zero in the long run, while such behavior is absent in the \mathcal{PT} -symmetric phase as well as in the unitary case.

The easiness of sampling the photon probability distribution for long times is not restricted to the present model and \mathcal{PT} -symmetric systems unless $\text{Im}(\lambda_{\max})$ is degenerate. Therefore, our result indicates that the long-time dynamical complexity transitions at which the distribution becomes easy to sample ubiquitously occur in postselected non-unitary quantum systems.

Discussion.— We note that it is not proved if the problem is classically hard in the red region of Fig. 1 (b). For example, as detailed in Supplemental Material [98], we can also analyze the long-time complexity transition through the rank of $W(t)$, which suggests that the time at which the problem becomes easy is smaller than t_{\max} . We conjecture that the classically hard regime exists in the red region, where $U(t)$ does not satisfy known conditions for computing and/or sampling the distribution to be easy [63, 85, 100]; indeed, $U(t)$ in the red region is typically full-rank, not sparse, and its components have various signs. However, We leave the detailed analysis for the red region as a future problem. In any case, the transitions characterized by $t_{\text{dis}}^{s/b}$ and t_{\max} are well-defined from the closeness of $P(\{n^{\text{in}}\}, \{n^{\text{out}}\}, t)$ to $P_{\text{dis}}(\{n^{\text{in}}\}, \{n^{\text{out}}\}, t)$ and $P_{\max}(\{n^{\text{out}}\})$, respectively.

While we have focused on sampling probability distributions of photons, computing $P_{\text{dis}}(\{n^{\text{in}}\}, \{n^{\text{out}}\}, t)$ for small t and $P_{\max}(\{n^{\text{out}}\})$ is also classically easy.

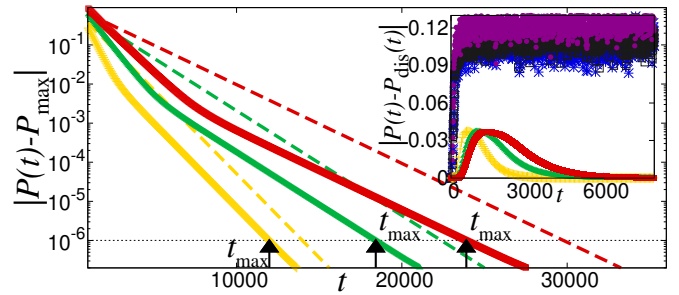


FIG. 3. L_1 -distance between $P(\{n^{\text{out}}\}, t)$ and $P_{\max}(\{n^{\text{out}}\})$ in Eq. (11). After the threshold time $t \geq t_{\max}$, $|P(t) - P_{\max}| < \delta$ and thus $P(\{n^{\text{out}}\}, t)$ becomes easy to sample efficiently through $P_{\max}(\{n^{\text{out}}\})$, which defines the long-time complexity transition. The dashed lines show $e^{-\Delta t}$, which confirms Eq. (12). The inset shows the same quantity as that in Fig. 2, which indicates an equivalence of $P_{\text{dis}}(\{n^{\text{out}}\}, t)$ and $P_{\max}(\{n^{\text{out}}\})$ in the long run for the \mathcal{PT} -broken phase. The blue, black, purples, yellow, green, and red symbols correspond to $e^\gamma = 1, 1.1, 1.2, 1.3, 1.4,$ and 1.5 , respectively. The initial condition and parameters are the same as those in Fig. 2.

The easiness for $P_{\text{dis}}(\{n^{\text{out}}\}, t)$ with the computational time $\mathcal{O}(n)$ is because the sum over ω in Eq. (6) is significantly simplified; that is, the matrix elements of $U(t)$ for small t almost vanish for the input and output states whose photon configurations are not spatially close. The easiness for computing $P_{\max}(\{n^{\text{out}}\})$ is due to the fact that it only takes $\mathcal{O}(M^3)$ computational time by numerically diagonalizing V .

We briefly discuss distinctions between our work and previous works on the lossy or non-unitary boson sampling problem in Refs. [82, 83, 87, 88]. While Refs. [82, 83, 87] considered the case where the number of photons decreases, our result shows that sampling photon distributions becomes easy in the \mathcal{PT} -broken phase even when the number of photons is conserved. Also, while the mechanism for the classically easy sampling is attributed to localization of photons in Ref. [88], it is due to the closeness between the actual distribution of photons and that for distinguishable particles in our work. Furthermore, the main result of our work, i.e., the transition associated with the computational complexity, was not discussed in Refs. [82, 83, 87, 88].

Conclusion.— We have shown that \mathcal{PT} symmetry breaking, a transition unique to open systems, drastically changes the complexity of the boson sampling problem in non-unitary dynamics. Regarding the short-time transition at which the distribution of photons deviates from that for distinguishable particles, \mathcal{PT} symmetry breaking prolongs the threshold time through the ballistic-diffusive transition of single-photon dynamics. Remarkably, \mathcal{PT} symmetry breaking leads to the additional long-time dynamical complexity transition at

which the problem becomes easy due to the dominant eigenstate, which is absent in isolated systems. This long-time transition appears in a wide range of non-unitary dynamics.

Our result bridges research areas about the complexity in quantum systems and non-unitarity in open systems. In addition, our result indicates that the non-unitarity can enhance classical computability of the boson sampling problem, unless \mathcal{PT} symmetry is present.

As future works, it should be interesting to explore the complexity in other types of open systems, such as many-body interacting systems and Markovian open systems described by Gorini–Kossakowski–Sudarshan–Lindblad master equation. It will also be intriguing to study relations between the transitions in open quantum systems and other indicators of the complexity, such as the entanglement entropy and quantum circuit complexity.

We thank Tomotaka Kuwahara, Hideaki Obuse, and Yutaka Shikano for fruitful discussions.

-
- [1] N. Hatano and D. R. Nelson, Localization transitions in non-Hermitian quantum mechanics, *Phys. Rev. Lett.* **77**, 570 (1996).
- [2] N. M. Shnerb and D. R. Nelson, Winding numbers, complex currents, and non-Hermitian localization, *Phys. Rev. Lett.* **80**, 5172 (1998).
- [3] J. Feinberg and A. Zee, Non-Hermitian localization and delocalization, *Phys. Rev. E* **59**, 6433 (1999).
- [4] S. Kalish, Z. Lin, and T. Kottos, Light transport in random media with \mathcal{PT} symmetry, *Phys. Rev. A* **85**, 055802 (2012).
- [5] A. Basiri, Y. Bromberg, A. Yamilov, H. Cao, and T. Kottos, Light localization induced by a random imaginary refractive index, *Phys. Rev. A* **90**, 043815 (2014).
- [6] K. Mochizuki and H. Obuse, Effects of disorder on non-unitary \mathcal{PT} symmetric quantum walks, *Interdisciplinary Information Sciences* **23**, 95 (2017).
- [7] R. Hamazaki, K. Kawabata, and M. Ueda, Non-Hermitian many-body localization, *Phys. Rev. Lett.* **123**, 090603 (2019).
- [8] R. Hamazaki, K. Kawabata, N. Kura, and M. Ueda, Universality classes of non-hermitian random matrices, *Phys. Rev. Research* **2**, 023286 (2020).
- [9] K. Mochizuki, N. Hatano, J. Feinberg, and H. Obuse, Statistical properties of eigenvalues of the non-Hermitian Su-Schrieffer-Heeger model with random hopping terms, *Phys. Rev. E* **102**, 012101 (2020).
- [10] L.-Z. Tang, L.-F. Zhang, G.-Q. Zhang, and D.-W. Zhang, Topological anderson insulators in two-dimensional non-hermitian disordered systems, *Phys. Rev. A* **101**, 063612 (2020).
- [11] A. F. Tzortzakakis, K. G. Makris, and E. N. Economou, Non-Hermitian disorder in two-dimensional optical lattices, *Phys. Rev. B* **101**, 014202 (2020).
- [12] X. Luo, T. Ohtsuki, and R. Shindou, Universality classes of the anderson transitions driven by non-hermitian disorder, *Phys. Rev. Lett.* **126**, 090402 (2021).
- [13] C. M. Bender and S. Boettcher, Real spectra in non-Hermitian Hamiltonians having \mathcal{PT} symmetry, *Phys. Rev. Lett.* **80**, 5243 (1998).
- [14] C. M. Bender, D. C. Brody, and H. F. Jones, Complex extension of quantum mechanics, *Phys. Rev. Lett.* **89**, 270401 (2002).
- [15] C. M. Bender, M. Berry, and A. Mandilara, Generalized \mathcal{PT} symmetry and real spectra, *Journal of Physics A: Mathematical and General* **35**, L467 (2002).
- [16] C. M. Bender, D. C. Brody, and H. F. Jones, Must a Hamiltonian be Hermitian?, *American Journal of Physics* **71**, 1095 (2003).
- [17] A. Mostafazadeh, Exact \mathcal{PT} -symmetry is equivalent to Hermiticity, *Journal of Physics A: Mathematical and General* **36**, 7081 (2003).
- [18] C. M. Bender, Making sense of non-Hermitian Hamiltonians, *Reports on Progress in Physics* **70**, 947 (2007).
- [19] A. Guo, G. J. Salamo, D. Duchesne, R. Morandotti, M. Volatier-Ravat, V. Aimez, G. A. Siviloglou, and D. N. Christodoulides, Observation of \mathcal{PT} -symmetry breaking in complex optical potentials, *Phys. Rev. Lett.* **103**, 093902 (2009).
- [20] C. E. Rüter, K. G. Makris, R. El-Ganainy, D. N. Christodoulides, M. Segev, and D. Kip, Observation of parity–time symmetry in optics, *Nature physics* **6**, 192 (2010).
- [21] Z. Lin, H. Ramezani, T. Eichelkraut, T. Kottos, H. Cao, and D. N. Christodoulides, Unidirectional invisibility induced by \mathcal{PT} -symmetric periodic structures, *Phys. Rev. Lett.* **106**, 213901 (2011).
- [22] N. M. Chtchelkatchev, A. A. Golubov, T. I. Baturina, and V. M. Vinokur, Stimulation of the fluctuation superconductivity by \mathcal{PT} symmetry, *Phys. Rev. Lett.* **109**, 150405 (2012).
- [23] M.-A. Miri, P. LiKamWa, and D. N. Christodoulides, Large area single-mode parity–time-symmetric laser amplifiers, *Optics letters* **37**, 764 (2012).
- [24] A. Regensburger, C. Bersch, M.-A. Miri, G. Onishchukov, D. N. Christodoulides, and U. Peschel, Parity–time synthetic photonic lattices, *Nature* **488**, 167 (2012).
- [25] B. Peng, Ş. K. Özdemir, F. Lei, F. Monifi, M. Gianfreda, G. L. Long, S. Fan, F. Nori, C. M. Bender, and L. Yang, Parity–time-symmetric whispering-gallery microcavities, *Nature Physics* **10**, 394 (2014).
- [26] L. Feng, Z. J. Wong, R.-M. Ma, Y. Wang, and X. Zhang, Single-mode laser by parity-time symmetry breaking, *Science* **346**, 972 (2014).
- [27] H. Hodaei, M.-A. Miri, M. Heinrich, D. N. Christodoulides, and M. Khajavikhan, Parity-time-symmetric microring lasers, *Science* **346**, 975 (2014).
- [28] K. Mochizuki, D. Kim, and H. Obuse, Explicit definition of \mathcal{PT} symmetry for nonunitary quantum walks with gain and loss, *Phys. Rev. A* **93**, 062116 (2016).
- [29] Y. Ashida, S. Furukawa, and M. Ueda, Parity-time-symmetric quantum critical phenomena, *Nature communications* **8**, 15791 (2017).
- [30] L. Xiao, X. Zhan, Z. Bian, K. Wang, X. Zhang, X. Wang, J. Li, K. Mochizuki, D. Kim, N. Kawakami, W. Yi, H. Obuse, B. C. Sanders, and P. Xue, Observation of topological edge states in parity–time-

- symmetric quantum walks, *Nature Physics* **13**, 1117 (2017).
- [31] S. Longhi, Parity-time symmetry meets photonics: A new twist in non-Hermitian optics, *EPL (Europhysics Letters)* **120**, 64001 (2018).
- [32] R. El-Ganainy, K. G. Makris, M. Khajavikhan, Z. H. Musslimani, S. Rotter, and D. N. Christodoulides, Non-Hermitian physics and PT symmetry, *Nature Physics* **14**, 11 (2018).
- [33] J. Li, A. K. Harter, J. Liu, L. de Melo, Y. N. Joglekar, and L. Luo, Observation of parity-time symmetry breaking transitions in a dissipative Floquet system of ultracold atoms, *Nature communications* **10**, 855 (2019).
- [34] S. Longhi, Non-Bloch \mathcal{PT} symmetry breaking in non-Hermitian photonic quantum walks, *Opt. Lett.* **44**, 5804 (2019).
- [35] M. Kawasaki, K. Mochizuki, N. Kawakami, and H. Obuse, Bulk-edge correspondence and dynamics of multiple edge states of a non-unitary three-step quantum walk with PT symmetry, *Progress of Theoretical and Experimental Physics* **ptaa034**, 10.1093/ptep/ptaa034 (2020).
- [36] K. Mochizuki, D. Kim, N. Kawakami, and H. Obuse, Bulk-edge correspondence in nonunitary Floquet systems with chiral symmetry, *Phys. Rev. A* **102**, 062202 (2020).
- [37] Y. Takasu, T. Yagami, Y. Ashida, R. Hamazaki, Y. Kuno, and Y. Takahashi, Pt-symmetric non-hermitian quantum many-body system using ultracold atoms in an optical lattice with controlled dissipation, *Progress of Theoretical and Experimental Physics* **2020**, 12A110 (2020).
- [38] K. Esaki, M. Sato, K. Hasebe, and M. Kohmoto, Edge states and topological phases in non-Hermitian systems, *Phys. Rev. B* **84**, 205128 (2011).
- [39] Y. C. Hu and T. L. Hughes, Absence of topological insulator phases in non-Hermitian pt -symmetric Hamiltonians, *Phys. Rev. B* **84**, 153101 (2011).
- [40] C. Poli, M. Bellec, U. Kuhl, F. Mortessagne, and H. Schomerus, Selective enhancement of topologically induced interface states in a dielectric resonator chain, *Nature communications* **6**, 6710 (2015).
- [41] T. E. Lee, Anomalous edge state in a non-Hermitian lattice, *Phys. Rev. Lett.* **116**, 133903 (2016).
- [42] M. A. Bandres, S. Wittek, G. Harari, M. Parto, J. Ren, M. Segev, D. N. Christodoulides, and M. Khajavikhan, Topological insulator laser: Experiments, *Science* **359**, eaar4005 (2018).
- [43] T. Chen, B. Wang, and X. Zhang, Characterization of topological phases and selection of topological interface modes in the parity-time-symmetric quantum walk, *Phys. Rev. A* **97**, 052117 (2018).
- [44] Z. Gong, Y. Ashida, K. Kawabata, K. Takasan, S. Higashikawa, and M. Ueda, Topological phases of non-Hermitian systems, *Phys. Rev. X* **8**, 031079 (2018).
- [45] G. Harari, M. A. Bandres, Y. Lumer, M. C. Rechtsman, Y. D. Chong, M. Khajavikhan, D. N. Christodoulides, and M. Segev, Topological insulator laser: theory, *Science* **359**, eaar4003 (2018).
- [46] F. K. Kunst, E. Edvardsson, J. C. Budich, and E. J. Bergholtz, Biorthogonal bulk-boundary correspondence in non-Hermitian systems, *Phys. Rev. Lett.* **121**, 026808 (2018).
- [47] M. Parto, S. Wittek, H. Hodaei, G. Harari, M. A. Bandres, J. Ren, M. C. Rechtsman, M. Segev, D. N. Christodoulides, and M. Khajavikhan, Edge-mode lasing in 1d topological active arrays, *Phys. Rev. Lett.* **120**, 113901 (2018).
- [48] S. Yao and Z. Wang, Edge states and topological invariants of non-Hermitian systems, *Phys. Rev. Lett.* **121**, 086803 (2018).
- [49] C. H. Lee and R. Thomale, Anatomy of skin modes and topology in non-Hermitian systems, *Phys. Rev. B* **99**, 201103(R) (2019).
- [50] K. Sone and Y. Ashida, Anomalous topological active matter, *Phys. Rev. Lett.* **123**, 205502 (2019).
- [51] F. Song, S. Yao, and Z. Wang, Non-hermitian skin effect and chiral damping in open quantum systems, *Phys. Rev. Lett.* **123**, 170401 (2019).
- [52] K. Yokomizo and S. Murakami, Non-Bloch band theory of non-Hermitian systems, *Phys. Rev. Lett.* **123**, 066404 (2019).
- [53] K. Kawabata, T. Bessho, and M. Sato, Classification of exceptional points and non-Hermitian topological semimetals, *Phys. Rev. Lett.* **123**, 066405 (2019).
- [54] K. Kawabata, K. Shiozaki, M. Ueda, and M. Sato, Symmetry and topology in non-Hermitian physics, *Phys. Rev. X* **9**, 041015 (2019).
- [55] T. Helbig, T. Hofmann, S. Imhof, M. Abdelghany, T. Kiessling, L. Molenkamp, C. Lee, A. Szameit, M. Greiter, and R. Thomale, Generalized bulk-boundary correspondence in non-hermitian topoelectrical circuits, *Nature Physics* **16**, 747 (2020).
- [56] N. Okuma, K. Kawabata, K. Shiozaki, and M. Sato, Topological origin of non-Hermitian skin effects, *Phys. Rev. Lett.* **124**, 086801 (2020).
- [57] K. Sone, Y. Ashida, and T. Sagawa, Exceptional non-Hermitian topological edge mode and its application to active matter, *Nature communications* **11**, 5745 (2020).
- [58] L. Xiao, T. Deng, K. Wang, G. Zhu, Z. Wang, W. Yi, and P. Xue, Non-Hermitian bulk-boundary correspondence in quantum dynamics, *Nature Physics* **16**, 761 (2020).
- [59] S. Weidemann, M. Kremer, T. Helbig, T. Hofmann, A. Stegmaier, M. Greiter, R. Thomale, and A. Szameit, Topological funneling of light, *Science* **368**, 311 (2020).
- [60] T. Haga, M. Nakagawa, R. Hamazaki, and M. Ueda, Liouvillian skin effect: Slowing down of relaxation processes without gap closing, *Phys. Rev. Lett.* **127**, 070402 (2021).
- [61] J.-S. Pan, L. Li, and J. Gong, Point-gap topology with complete bulk-boundary correspondence and anomalous amplification in the fock space of dissipative quantum systems, *Phys. Rev. B* **103**, 205425 (2021).
- [62] J.-S. Tang, Y.-T. Wang, S. Yu, D.-Y. He, J.-S. Xu, B.-H. Liu, G. Chen, Y.-N. Sun, K. Sun, Y.-J. Han, et al., Experimental investigation of the no-signalling principle in parity-time symmetric theory using an open quantum system, *Nature Photonics* **10**, 642 (2016).
- [63] S. Aaronson and A. Arkhipov, The computational complexity of linear optics, *Proceedings of the forty-third annual ACM symposium on Theory of computing*, 333 (2011).
- [64] S. Aaronson and A. Arkhipov, The computational complexity of linear optics, *Theory of Computing* **9**, 143 (2013).
- [65] M. A. Broome, A. Fedrizzi, S. Rahimi-Keshari, J. Dove,

- S. Aaronson, T. C. Ralph, and A. G. White, Photonic boson sampling in a tunable circuit, *Science* **339**, 794 (2013).
- [66] A. Crespi, R. Osellame, R. Ramponi, D. J. Brod, E. F. Galvao, N. Spagnolo, C. Vitelli, E. Maiorino, P. Mataloni, and F. Sciarrino, Integrated multimode interferometers with arbitrary designs for photonic boson sampling, *Nature photonics* **7**, 545 (2013).
- [67] J. B. Spring, B. J. Metcalf, P. C. Humphreys, W. S. Kolthammer, X.-M. Jin, M. Barbieri, A. Datta, N. Thomas-Peter, N. K. Langford, D. Kundys, J. C. Gates, B. J. Smith, P. G. R. Smith, and I. A. Walmsley, Boson sampling on a photonic chip, *Science* **339**, 798 (2013).
- [68] M. Tillmann, B. Dakić, R. Heilmann, S. Nolte, A. Szameit, and P. Walther, Experimental boson sampling, *Nature photonics* **7**, 540 (2013).
- [69] A. P. Lund, A. Laing, S. Rahimi-Keshari, T. Rudolph, J. L. O'Brien, and T. C. Ralph, Boson sampling from a gaussian state, *Phys. Rev. Lett.* **113**, 100502 (2014).
- [70] M. C. Tichy, K. Mayer, A. Buchleitner, and K. Mølmer, Stringent and efficient assessment of boson-sampling devices, *Phys. Rev. Lett.* **113**, 020502 (2014).
- [71] K. P. Seshadreesan, J. P. Olson, K. R. Motes, P. P. Rohde, and J. P. Dowling, Boson sampling with displaced single-photon fock states versus single-photon-added coherent states: The quantum-classical divide and computational-complexity transitions in linear optics, *Phys. Rev. A* **91**, 022334 (2015).
- [72] S. Rahimi-Keshari, A. P. Lund, and T. C. Ralph, What can quantum optics say about computational complexity theory?, *Phys. Rev. Lett.* **114**, 060501 (2015).
- [73] S. Aaronson and D. J. Brod, Bosonsampling with lost photons, *Phys. Rev. A* **93**, 012335 (2016).
- [74] L. Latmiral, N. Spagnolo, and F. Sciarrino, Towards quantum supremacy with lossy scattershot boson sampling, *New Journal of Physics* **18**, 113008 (2016).
- [75] S. Rahimi-Keshari, T. C. Ralph, and C. M. Caves, Sufficient conditions for efficient classical simulation of quantum optics, *Phys. Rev. X* **6**, 021039 (2016).
- [76] C. S. Hamilton, R. Kruse, L. Sansoni, S. Barkhofen, C. Silberhorn, and I. Jex, Gaussian boson sampling, *Phys. Rev. Lett.* **119**, 170501 (2017).
- [77] Y. He, X. Ding, Z.-E. Su, H.-L. Huang, J. Qin, C. Wang, S. Unsleber, C. Chen, H. Wang, Y.-M. He, X.-L. Wang, W.-J. Zhang, S.-J. Chen, C. Schneider, M. Kamp, L.-X. You, Z. Wang, S. Höfling, C.-Y. Lu, and J.-W. Pan, Time-bin-encoded boson sampling with a single-photon device, *Phys. Rev. Lett.* **118**, 190501 (2017).
- [78] J. C. Loredó, M. A. Broome, P. Hilaire, O. Gazzano, I. Sagnes, A. Lemaitre, M. P. Almeida, P. Senellart, and A. G. White, Boson sampling with single-photon fock states from a bright solid-state source, *Phys. Rev. Lett.* **118**, 130503 (2017).
- [79] A. Neville, C. Sparrow, R. Clifford, E. Johnston, P. M. Birchall, A. Montanaro, and A. Laing, Classical boson sampling algorithms with superior performance to near-term experiments, *Nature Physics* **13**, 1153 (2017).
- [80] H. Wang, Y. He, Y.-H. Li, Z.-E. Su, B. Li, H.-L. Huang, X. Ding, M.-C. Chen, C. Liu, J. Qin, J.-P. Li, Y.-M. He, C. Schneider, M. Kamp, C.-Z. Peng, S. Höfling, C.-Y. Lu, and J.-W. Pan, High-efficiency multiphoton boson sampling, *Nature Photonics* **11**, 361 (2017).
- [81] A. Deshpande, B. Fefferman, M. C. Tran, M. Foss-Feig, and A. V. Gorshkov, Dynamical phase transitions in sampling complexity, *Phys. Rev. Lett.* **121**, 030501 (2018).
- [82] M. Oszmaniec and D. J. Brod, Classical simulation of photonic linear optics with lost particles, *New Journal of Physics* **20**, 092002 (2018).
- [83] R. García-Patrón, J. J. Renema, and V. Shchesnovich, Simulating boson sampling in lossy architectures, *Quantum* **3**, 169 (2019).
- [84] G. Muraleedharan, A. Miyake, and I. H. Deutsch, Quantum computational supremacy in the sampling of bosonic random walkers on a one-dimensional lattice, *New Journal of Physics* **21**, 055003 (2019).
- [85] W. Roga and M. Takeoka, Classical simulation of boson sampling with sparse output, *Scientific reports* **10**, 1 (2020).
- [86] H.-S. Zhong, H. Wang, Y.-H. Deng, M.-C. Chen, L.-C. Peng, Y.-H. Luo, J. Qin, D. Wu, X. Ding, Y. Hu, P. Hu, X.-Y. Yang, W.-J. Zhang, H. Li, Y. Li, X. Jiang, L. Gan, G. Yang, L. You, Z. Wang, L. Li, N.-L. Liu, C.-Y. Lu, and J.-W. Pan, Quantum computational advantage using photons, *Science* **370**, 1460 (2020).
- [87] C. Oh, K. Noh, B. Fefferman, and L. Jiang, Classical simulation of lossy boson sampling using matrix product operators, *Phys. Rev. A* **104**, 022407 (2021).
- [88] X. Chen, Non-unitary free boson dynamics and the boson sampling problem, arXiv preprint arXiv:2110.12230 (2021).
- [89] Y. Omar, N. Paunković, L. Sheridan, and S. Bose, Quantum walk on a line with two entangled particles, *Phys. Rev. A* **74**, 042304 (2006).
- [90] P. K. Pathak and G. S. Agarwal, Quantum random walk of two photons in separable and entangled states, *Phys. Rev. A* **75**, 032351 (2007).
- [91] A. Peruzzo, M. Lobino, J. C. Matthews, N. Matsuda, A. Politi, K. Poulios, X.-Q. Zhou, Y. Lahini, N. Ismail, K. Wörhoff, Y. Bromberg, Y. Silberberg, M. G. Thompson, and J. L. O'Brien, Quantum walks of correlated photons, *Science* **329**, 1500 (2010).
- [92] K. Mayer, M. C. Tichy, F. Mintert, T. Konrad, and A. Buchleitner, Counting statistics of many-particle quantum walks, *Phys. Rev. A* **83**, 062307 (2011).
- [93] A. Schreiber, A. Gábris, P. P. Rohde, K. Laiho, M. Štefaňák, V. Potoček, C. Hamilton, I. Jex, and C. Silberhorn, A 2d quantum walk simulation of two-particle dynamics, *Science* **336**, 55 (2012).
- [94] F. Cardano, F. Massa, H. Qassim, E. Karimi, S. Slussarenko, D. Paparo, C. de Lisio, F. Sciarrino, E. Santamato, R. W. Boyd, and L. Marrucci, Quantum walks and wavepacket dynamics on a lattice with twisted photons, *Science advances* **1**, e1500087 (2015).
- [95] Q. Wang and Z.-J. Li, Repelling, binding, and oscillating of two-particle discrete-time quantum walks, *Annals of Physics* **373**, 1 (2016).
- [96] C. Esposito, M. R. Barros, A. Durán Hernández, G. Carvacho, F. Di Colandrea, R. Barboza, F. Cardano, N. Spagnolo, L. Marrucci, and F. Sciarrino, Quantum walks of two correlated photons in a 2d synthetic lattice, *npj Quantum Information* **8**, 34 (2022).
- [97] K. Wang, X. Qiu, L. Xiao, X. Zhan, Z. Bian, B. C. Sanders, W. Yi, and P. Xue, Observation of emergent momentum-time skyrmions in parity-time-symmetric non-unitary quench dynamics, *Nature communications*

- 10**, 2293 (2019).
- [98] See Supplemental Material for the derivation of non-unitary dynamics, \mathcal{PT} symmetry breaking, ballistic and diffusive behaviors, and estimations for threshold times, which includes Refs. [101–106].
- [99] S. Scheel, Permanents in linear optical networks, arXiv preprint quant-ph/0406127 (2004).
- [100] A. I. Barvinok, Two algorithmic results for the traveling salesman problem, *Mathematics of Operations Research* **21**, 65 (1996).
- [101] B. Do, M. L. Stohler, S. Balasubramanian, D. S. Elliott, C. Eash, E. Fischbach, M. A. Fischbach, A. Mills, and B. Zwickl, Experimental realization of a quantum quincunx by use of linear optical elements, *JOSA B* **22**, 499 (2005).
- [102] M. A. Broome, A. Fedrizzi, B. P. Lanyon, I. Kassal, A. Aspuru-Guzik, and A. G. White, Discrete single-photon quantum walks with tunable decoherence, *Phys. Rev. Lett.* **104**, 153602 (2010).
- [103] T. Kitagawa, M. A. Broome, A. Fedrizzi, M. S. Rudner, E. Berg, I. Kassal, A. Aspuru-Guzik, E. Demler, and A. G. White, Observation of topologically protected bound states in photonic quantum walks, *Nature communications* **3**, 882 (2012).
- [104] Y.-y. Zhao, N.-k. Yu, P. Kurzyński, G.-y. Xiang, C.-F. Li, and G.-C. Guo, Experimental realization of generalized qubit measurements based on quantum walks, *Phys. Rev. A* **91**, 042101 (2015).
- [105] F. Cardano, M. Maffei, F. Massa, B. Piccirillo, C. De Lisio, G. De Filippis, V. Cataudella, E. Santamato, and L. Marrucci, Statistical moments of quantum-walk dynamics reveal topological quantum transitions, *Nature communications* **7**, 11439 (2016).
- [106] X.-Y. Xu, Q.-Q. Wang, S.-J. Tao, W.-W. Pan, Z. Chen, M. Jan, Y.-T. Zhan, K. Sun, J.-S. Xu, Y.-J. Han, C.-F. Li, and G.-C. Guo, Experimental classification of quenched quantum walks by dynamical chern number, *Phys. Rev. Research* **1**, 033039 (2019).

Supplemental Material for “Complexity Transitions in Non-Unitary Boson Sampling Dynamics”

Ken Mochizuki¹ and Ryusuke Hamazaki^{1,2}

¹*Nonequilibrium Quantum Statistical Mechanics RIKEN Hakubi Research Team,
RIKEN Cluster for Pioneering Research (CPR), 2-1 Hirosawa, Wako 351-0198, Japan*

²*RIKEN Interdisciplinary Theoretical and Mathematical Sciences Program (iTHEMS), 2-1 Hirosawa, Wako 351-0198, Japan*

S1. COMPONENTS OF V REALIZED BY OPTICAL ELEMENTS AND POSTSELECTIONS

We here discuss that our model describes postselected non-unitary dynamics of photons passing through optical elements.

First, we explain the effects of optical elements that do not change the number of photons and lead to unitary dynamics observed in Refs. [1–6]. A wave plate, described by a shallow purple rectangle in Fig. S1, changes the polarization of photons. We consider the case in which polarizations are altered by rotation matrices parametrized by angles θ as

$$\hat{C}(\theta) = \exp \left[\theta \sum_{x=1}^L (\hat{b}_{x,h}^\dagger \hat{b}_{x,v} - \hat{b}_{x,v}^\dagger \hat{b}_{x,h}) \right]. \quad (\text{S1})$$

The unitary transformation of creation operators by $\hat{C}(\theta)$ becomes

$$\begin{bmatrix} \hat{C}(\theta) \hat{b}_{x,h}^\dagger \hat{C}^\dagger(\theta) \\ \hat{C}(\theta) \hat{b}_{x,v}^\dagger \hat{C}^\dagger(\theta) \end{bmatrix} = \begin{bmatrix} \cos(\theta) & -\sin(\theta) \\ \sin(\theta) & \cos(\theta) \end{bmatrix} \begin{bmatrix} \hat{b}_{x,h}^\dagger \\ \hat{b}_{x,v}^\dagger \end{bmatrix}. \quad (\text{S2})$$

A beam displacer, corresponding to a thick green rectangle, shifts the positions of photons depending on their polarizations, as depicted in Fig. S1. We consider the case in which photons with the horizontal (h) and vertical (v) polarizations are shifted to the right and left directions, respectively. We can describe such effects by beam displacers utilizing an operator \hat{S} defined as

$$\begin{aligned} \hat{S} = & \exp \left[-i \frac{\pi}{2} \sum_{x=1}^L (\hat{b}_{x,h}^\dagger \hat{b}_{x,v} + \hat{b}_{x,v}^\dagger \hat{b}_{x,h}) \right] \\ & \times \exp \left[i \frac{\pi}{2} \sum_{x=1}^L (\hat{b}_{x+1,v}^\dagger \hat{b}_{x,h} + \hat{b}_{x-1,h}^\dagger \hat{b}_{x,v}) \right]. \quad (\text{S3}) \end{aligned}$$

Actually, by the operation of \hat{S} , creation operators are transformed as

$$\begin{pmatrix} \hat{S} \hat{b}_{x,h}^\dagger \hat{S}^\dagger \\ \hat{S} \hat{b}_{x,v}^\dagger \hat{S}^\dagger \end{pmatrix} = \begin{pmatrix} \hat{b}_{x+1,h}^\dagger \\ \hat{b}_{x-1,v}^\dagger \end{pmatrix}, \quad (\text{S4})$$

which corresponds to the position shifts of photons depending on their polarizations.

Second, we introduce how photons experience non-unitary dynamics, observed in Refs. [7, 8], on the basis of the combination of the postselection and an optical

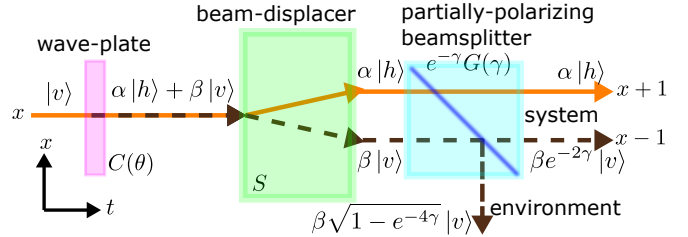


FIG. S1. Schematic picture for dynamics in which photons pass through optical elements. This figure corresponds to a sequence $G(+\gamma)SC(\theta)$ in terms of the matrices in Eq. (2). When photons with the polarization v pass through the wave plate, which is described as the shallow purple rectangle, the superposition of h and v is realized with $\alpha = -\sin(\theta)$ and $\beta = \cos(\theta)$. The beam displacer, which corresponds to the thick green rectangle, causes the position shift of photons depending on their polarization; photons with h and v respectively go to the right and left. When photons enter the partially polarizing beam splitter, which is the blue square, photons with v get into the environment with a probability $1 - e^{-4\gamma}$, while photons with h always go straight and remain in the system. If we carry out the postselection and focus only on the cases in which all photons are in the system, the creation operators for photons with v acquire the additional factor $e^{-2\gamma}$. While unitary dynamics by $C(\theta)$ and S is realized by photons passing through linear optical elements, couplings to environment and postselection are additionally needed for non-unitary dynamics by $G(\gamma)$.

element referred to as a partially polarizing beam splitter. The operation of photons by the partially polarizing beam splitter depends on the polarization. For simplicity, we explain effects of partially polarizing beam splitters for v , but we can easily understand effects of partially polarizing beam splitters for h by replacing v with h . If photons pass through the partially polarizing beam splitter for v , schematically described by the blue square in Fig. S1, photons with v are lost into the environment with a certain probability, while photons with h always remain in the system. Such processes can be described by

$$\hat{P}_v(\zeta) = \exp \left[\zeta \sum_{x=1}^L (\hat{b}_{s,x,v}^\dagger \hat{b}_{e,x,v} - \hat{b}_{e,x,v}^\dagger \hat{b}_{s,x,v}) \right] \quad (\text{S5})$$

where the subscripts s and e denote the system and environment, respectively. For photons with v in the system, $\hat{P}_v(\zeta)$ gives an outcome similar to that of $\hat{C}(\theta)$,

while the bases are mixed for s and e instead of h and v . If $\hat{P}_v(\zeta)$ acts on a state $|\psi_{\text{in}}\rangle = \prod_{x=x_1}^{x_n} [c_x \hat{b}_{s,x,h}^\dagger + d_x \hat{b}_{s,x,v}^\dagger] |s0\rangle \otimes |e0\rangle$ with c_x and d_x being complex coefficients, the output becomes

$$\begin{aligned} |\psi_{\text{out}}\rangle &= \hat{P}_v(\zeta) |\psi_{\text{in}}\rangle \\ &= \prod_{x=x_1}^{x_n} [c_x \hat{b}_{s,x,h}^\dagger + d_x \{\cos(\zeta) \hat{b}_{s,x,v}^\dagger - \sin(\zeta) \hat{b}_{e,x,v}^\dagger\}] |s0, e0\rangle, \end{aligned} \quad (\text{S6})$$

where $|s0\rangle$ and $|e0\rangle$ are the vacuum for the system and environment, respectively. Note that $|s0\rangle$ in Supplemental Material corresponds to $|0\rangle$ in the main text. The output state in Eq. (S6) includes states where photons are present in the environment, while the input state $|\psi_{\text{in}}\rangle$ only includes states where photons are absent in the environment and all photons exist in the system. We carry out the postselection for the state $|e0\rangle$. This corresponds to focusing only on cases in which all photons remain in the system. After the postselection, the state of the system becomes

$$\begin{aligned} |\psi_{\text{selected}}\rangle &\propto \langle e0 | \psi_{\text{out}} \rangle \\ &= \prod_{x=x_1}^{x_n} [c_x \hat{b}_{s,x,h}^\dagger + e^{-2\gamma} d_x \hat{b}_{s,x,v}^\dagger] |s0\rangle, \end{aligned} \quad (\text{S7})$$

where we put $e^{-2\gamma} = \cos(\zeta)$ with introducing a real and positive quantity γ . Therefore, by the partially polarizing beam splitter and the postselection to states with no photon in the environment, the creation operators are transformed as

$$\begin{aligned} \hat{P}_v[\zeta = \cos^{-1}(e^{-2\gamma})] \&\text{ postselection :} \\ \begin{pmatrix} \hat{b}_{x,h}^\dagger \\ \hat{b}_{x,v}^\dagger \end{pmatrix} &\rightarrow e^{-\gamma} \begin{pmatrix} e^{+\gamma} & 0 \\ 0 & e^{-\gamma} \end{pmatrix} \begin{pmatrix} \hat{b}_{x,h}^\dagger \\ \hat{b}_{x,v}^\dagger \end{pmatrix}. \end{aligned} \quad (\text{S8})$$

In the main text, we ignore the overall factor $e^{-\gamma}$ since it has no huge effect on dynamics, while it decreases the success probability of postselected dynamics. Thus, we introduce the matrix $\exp(\gamma\sigma_3)$, which includes the effective amplification of photons with h and is useful for analyzing \mathcal{PT} symmetry breaking. This corresponds to the non-unitary matrix $G(\gamma)$ in the main text. Note that $x_p = x_q$ with $p \neq q$ is allowed for $\prod_{x=x_1}^{x_n}$ in Eqs. (S6) and (S7). Thus, the above discussion can be applied to cases where several photons exist at a position x .

S2. \mathcal{PT} SYMMETRY AND ITS BREAKING

\mathcal{PT} symmetry for a time-evolution operator V is defined as

$$(\mathcal{PT})V(\mathcal{PT})^{-1} = V^{-1}, \quad (\text{S9})$$

where the symmetry operator \mathcal{PT} includes the complex conjugation \mathcal{K} . When V respects \mathcal{PT} symmetry, there

are two cases regarding its eigenstates,

$$V |\phi_l^{\text{R}}\rangle = \lambda_l |\phi_l^{\text{R}}\rangle, \quad \langle \phi_l^{\text{L}} | V = \lambda_l \langle \phi_l^{\text{L}} |, \quad (\text{S10})$$

where λ_l with $l = 1, 2, \dots, M$ is an eigenvalue of V and the eigenstates are bi-orthogonal as $\langle \phi_l^{\text{L}} | \phi_m^{\text{R}} \rangle = \delta_{lm}$. When an eigenstate $|\phi_l^{\text{L/R}}\rangle$ satisfies \mathcal{PT} symmetry, we have $|\lambda_l| = 1$, while \mathcal{PT} symmetry breaking of $|\phi_l^{\text{L/R}}\rangle$ results in $|\lambda_l| \neq 1$, namely

$$\begin{cases} \mathcal{PT} |\phi_l^{\text{L/R}}\rangle = |\phi_l^{\text{L/R}}\rangle \rightarrow |\lambda_l| = 1, \\ \mathcal{PT} |\phi_l^{\text{L/R}}\rangle \neq |\phi_l^{\text{L/R}}\rangle \rightarrow |\lambda_l| \neq 1. \end{cases} \quad (\text{S11})$$

Here, the equality for the eigenstate is satisfied up to a phase factor. These two different behaviors define the \mathcal{PT} -symmetric and \mathcal{PT} -broken phases. In the \mathcal{PT} -symmetric phase, all eigenstates respect \mathcal{PT} symmetry, and all eigenvalues satisfy $|\lambda_l| = 1$. In the \mathcal{PT} -broken phase, some of the eigenstates break \mathcal{PT} symmetry, and some eigenvalues deviate from the unit circle. While we have explained \mathcal{PT} symmetry for time-evolution operators and their eigenstates, this can be translated to Hamiltonians as $(\mathcal{PT})H(\mathcal{PT})^{-1} = H$ through $V = e^{-iH}$. In this case, $|\lambda_l| = 1$ in the \mathcal{PT} -symmetric phase and $|\lambda_l| \neq 1$ in the \mathcal{PT} -broken phase correspond to $\varepsilon_l \in \mathbb{R}$ and $\varepsilon_l \in \mathbb{C}$, respectively, where quasi-energies $\{\varepsilon_l = i \log(\lambda_l)\}$ are eigenvalues of the Hamiltonian $H = i \log(V)$ [9]. In many cases, \mathcal{PT} -symmetric systems experience transitions from the \mathcal{PT} -symmetric phase to the \mathcal{PT} -broken phase as a parameter is altered.

In systems with translational invariance, we consider \mathcal{PT} symmetry and eigen-equations in momentum space through the Fourier transformation. When a \mathcal{PT} symmetry operator is written as $\mathcal{PT} = \sum_x |-x\rangle \langle x| \otimes \Omega$ with Ω acting on internal states, Eq. (S9) corresponds to

$$\Omega \tilde{V}(k) \Omega^{-1} = \tilde{V}^{-1}(k), \quad (\text{S12})$$

which results in $\Omega \tilde{H}(k) \Omega^{-1} = \tilde{H}(k)$ with $\tilde{H}(k) = i \log[\tilde{V}(k)]$. In the present model $\tilde{V}(k)$ becomes

$$\tilde{V}(k) = e^{-i\frac{\theta_1}{2}\sigma_2} e^{(ik+\gamma)\sigma_3} e^{-i\theta_2\sigma_2} e^{(ik-\gamma)\sigma_3} e^{-i\frac{\theta_1}{2}\sigma_2}, \quad (\text{S13})$$

and we can easily confirm Eq. (S12) with $\Omega = \sigma_3 \mathcal{K}$ through $\sigma_3 (e^{-i\theta\sigma_2})^* \sigma_3 = e^{+i\theta\sigma_2}$, $\sigma_3 (e^{+ik\sigma_3})^* \sigma_3 = e^{-ik\sigma_3}$, and $\sigma_3 (e^{\gamma\sigma_3})^* \sigma_3 = e^{\gamma\sigma_3}$ [9]. The eigenvalues are labeled by momentum k and band indices $s = \pm$, where eigen-equations become

$$\tilde{V}(k) |\phi_{\pm}^{\text{R}}(k)\rangle = \lambda_{\pm}(k) |\phi_{\pm}^{\text{R}}(k)\rangle, \quad (\text{S14})$$

$$\langle \phi_{\pm}^{\text{L}}(k) | \tilde{V}(k) = \langle \phi_{\pm}^{\text{L}}(k) | \lambda_{\pm}(k). \quad (\text{S15})$$

The relation between \mathcal{PT} symmetry of eigenstates and the absolute values of eigenvalues is the same as Eq. (S11), where \mathcal{PT} is replaced with Ω and the label becomes $l = (k, s)$. The eigenvalues of $\tilde{V}(k)$ become

$$\lambda_{\pm}(k) = e^{-i\varepsilon_{\pm}(k)} = d(k) \pm \sqrt{d^2(k) - 1}, \quad (\text{S16})$$

where $d(k)$ is defined as $d(k) = \cos(\theta_1) \cos(\theta_2) \cos(2k) - \sin(\theta_1) \sin(\theta_2) \cosh(2\gamma)$. Figure S2 shows the real and imaginary parts of the quasi-energies with $\theta_1 = 0.65\pi$ and $\theta_2 = 0.25\pi$. When the dissipation is weak as in Fig. S2 (b), all eigenstates preserve \mathcal{PT} symmetry and thus $\varepsilon_{\pm}(k)$ have no imaginary part for arbitrary k , similar to the unitary case in (a). When the value of γ is large, some of the eigenstates break \mathcal{PT} symmetry, resulting in non-zero imaginary parts of $\varepsilon_{\pm}(k)$ for some k , which is shown in Fig. S2 (c). Since $\cos(\theta_1) \cos(\theta_2) < 0$ and $\sin(\theta_1) \sin(\theta_2) > 0$, the threshold value $\gamma_{\mathcal{PT}}$ for \mathcal{PT} symmetry breaking is determined through $\lambda_-(k=0) = -1$, and we can obtain $\gamma_{\mathcal{PT}} = \cosh^{-1} \{ [1 + \cos(\theta_1) \cos(\theta_2)] / \sin(\theta_1) \sin(\theta_2) \} / 2$, which leads to $e^{\gamma_{\mathcal{PT}}} \simeq 1.22$. We note that the present model satisfies particle-hole symmetry $\tilde{V}^*(k) = \tilde{V}(-k)$ and thus $\varepsilon_{\pm}(k) = -\varepsilon_{\pm}^*(k)$, while this symmetry is not crucial to the transitions.

S3. TRANSITION BETWEEN BALLISTIC AND DIFFUSIVE DYNAMICS DUE TO \mathcal{PT} SYMMETRY BREAKING

We explain that \mathcal{PT} symmetry breaking causes the transition from ballistic dynamics into diffusive dynamics for a single photon. As revealed in the next section, the ballistic-diffusive transition profoundly affects the complexity transition in short-time dynamics.

Calculating the moments of x , we derive the ballistic-diffusive transition caused by \mathcal{PT} symmetry breaking. With the initial state $|\psi(t=0)\rangle = |x^{\text{in}}=0\rangle \otimes |\sigma^{\text{in}}\rangle$, the m th-order moment can be written as

$$\begin{aligned} \langle x^m(t) \rangle &= \frac{(-i)^m}{N(t)} \int_{-\pi}^{\pi} dk \langle \sigma^{\text{in}} | [\tilde{V}^\dagger(k)]^t \frac{d^m}{dk^m} \tilde{V}^t(k) | \sigma^{\text{in}} \rangle \\ &\simeq \frac{(-i)^m}{N(t)} \int_{-\pi}^{\pi} dk \sum_s f_s(k) e^{i\varepsilon_s^*(k)t} \frac{d^m e^{-i\varepsilon_s(k)t}}{dk^m} \end{aligned} \quad (\text{S17})$$

where $f_s(k) = |\langle \phi_s^{\text{L}}(k) | \sigma^{\text{in}} \rangle|^2 \langle \phi_s^{\text{R}}(k) | \phi_s^{\text{R}}(k) \rangle$ and $N(t)$ is the normalization factor

$$N(t) = \int_{-\pi}^{\pi} dk \langle \sigma^{\text{in}} | [V^\dagger(k)]^t \tilde{V}^t(k) | \sigma^{\text{in}} \rangle. \quad (\text{S18})$$

Here, we have used the eigenvalue decomposition of $\tilde{V}^t(k)$

$$\begin{aligned} \tilde{V}^t(k) &= \exp[-i\tilde{H}(k)t] \\ &= \sum_s e^{-i\varepsilon_s(k)t} |\phi_s^{\text{R}}(k)\rangle \langle \phi_s^{\text{L}}(k)| \end{aligned} \quad (\text{S19})$$

with $s = \pm$. In deriving the second line of Eq. (S17), we focus on the leading terms for large t , where the sign for the integrand is independent of k . This is because the other terms should be negligibly small due to the cancellation caused by the oscillation of the integrand as we sweep the Brillouin zone.

First, we show the ballistic behavior in the \mathcal{PT} -symmetric phase by calculating the variance of x . In the

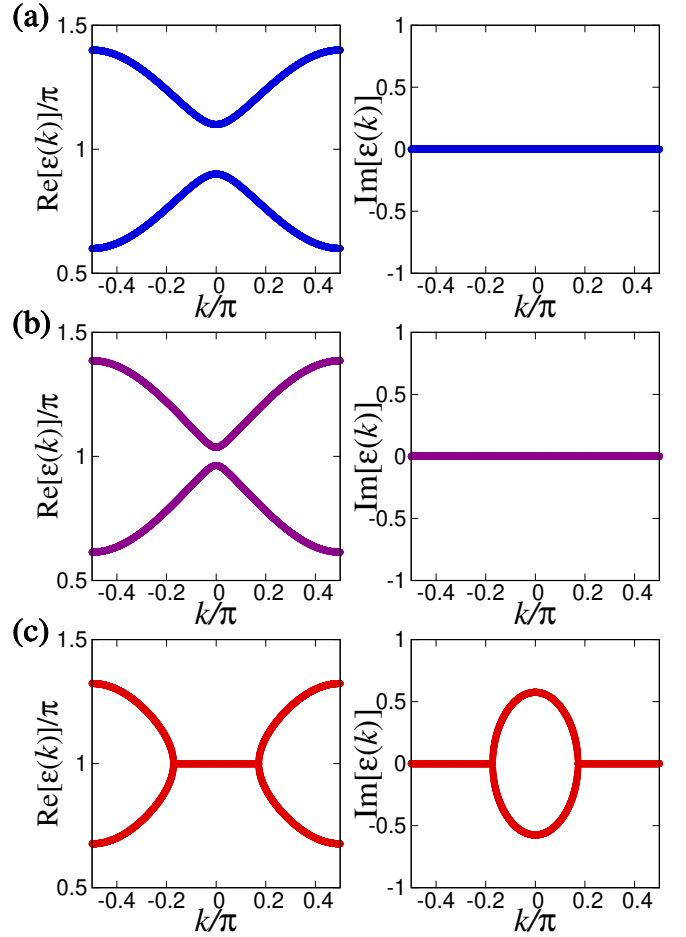


FIG. S2. Quasi-energy dispersion relations of $\tilde{V}(k)$ with $\theta_1 = 0.65\pi$, $\theta_2 = 0.25\pi$, (a) $e^\gamma = 1$ where $\tilde{V}(k)$ is unitary, (b) $e^\gamma = 1.2$ in the \mathcal{PT} -symmetric phase, and (c) $e^\gamma = 1.5$ in the \mathcal{PT} -broken phase. Some quasi-energies have non-zero imaginary parts in the \mathcal{PT} -broken phase, while all quasi-energies are real in the \mathcal{PT} -symmetric phase. In the \mathcal{PT} -broken phase, we can approximate $\varepsilon_{\pm}(k)$ by a quadratic function without a linear term as in Eq. (S21) near $k=0$ owing to $\frac{d\varepsilon_{\pm}(k)}{dk} = 0$ at this point.

\mathcal{PT} -symmetric phase, the dominant term in the variance reads

$$\langle x^2(t) \rangle - \langle x(t) \rangle^2 \simeq t^2 \frac{\int_{-\pi}^{\pi} dk \sum_s \left[\frac{d\varepsilon_s(k)}{dk} \right]^2 f_s(k)}{\int_{-\pi}^{\pi} dk \sum_s f_s(k)}. \quad (\text{S20})$$

Equation (S20) indicates that dynamics is ballistic, since the coefficient of t^2 is always positive. Actually, as shown in Fig. S3 (b), single-photon dynamics exhibits the ballistic behavior, similar to the unitary case in Fig. S3 (a).

Second, we show that dynamics becomes diffusive in the \mathcal{PT} -broken phase, i.e., the single-photon distribution asymptotically becomes the Gaussian distribution. To see this, we focus only on $|\phi_{\pm}^{\text{L/R}}(k)\rangle$ around $k=0$

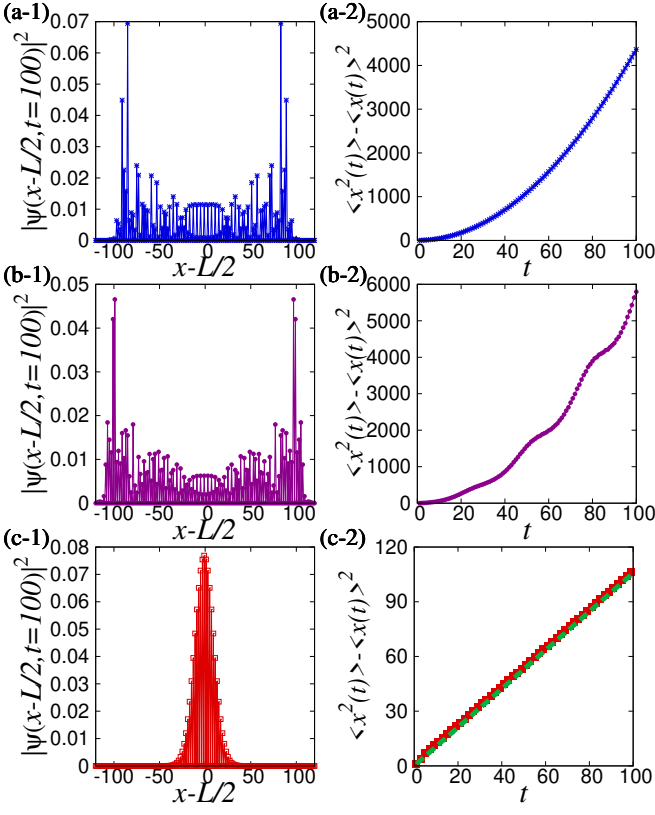


FIG. S3. Single-photon dynamics of quantum walks where $\theta_1 = 0.65\pi$, $\theta_2 = 0.25\pi$, and $|\psi(t=0)\rangle = |x^{\text{in}} = L/2\rangle \otimes |\sigma^{\text{in}}\rangle$ with $|\sigma^{\text{in}}\rangle = (|h\rangle + i|v\rangle)/\sqrt{2}$. The parameters for the dissipation are (a) $e^\gamma = 1$, (b) $e^\gamma = 1.2$, and (c) $e^\gamma = 1.5$. In the left column, the single-photon probability distributions at $t = 100$ are shown. In the right column, the variance of x is displayed as a function of time. In (b) \mathcal{PT} -symmetric and (c) \mathcal{PT} -broken phases, dynamics becomes ballistic and diffusive, respectively. In (c-2), the analytically derived variance $Dt/2$ described by the green broken line agrees well with the numerical result described by the red squares.

since these growing states become dominant over the other states. Since $\text{Re}[\varepsilon_-(k)] = 0$ around $k = 0$ and $\frac{d}{dk}\varepsilon_-(k) = 0$ at $k = 0$, as demonstrated in Fig. S2 (c), we can approximate the dispersion relation of the quasi-energy as

$$\varepsilon_-(k) \simeq \varepsilon_-(k=0) - i\frac{D}{2}k^2 \quad (\text{S21})$$

where the coefficient of k^2 becomes $D = \left| \frac{d^2}{dk^2}\varepsilon_-(k) \right|_{k=0} = |4\cos(\theta_1)\cos(\theta_2)/\sqrt{d^2(k=0)-1}|$. We note that such an approximation is applicable in a wide range of \mathcal{PT} -symmetric non-Hermitian systems with translation invariance. This is because such systems exhibit dispersion relations similar to that in Fig. S2 (c) if some of the eigenstates break \mathcal{PT} symmetry. Therefore, the diffusive behavior which we explain below can be observed in a wide range of \mathcal{PT} -symmetric systems.

On the basis of Eqs. (S17) and (S21), the m th moment of x in the \mathcal{PT} -broken phase becomes

$$\begin{aligned} \langle x^m(t) \rangle &\simeq \frac{(-i)^m \int_{-\infty}^{+\infty} dk e^{-\frac{Dk^2}{2}t} \frac{d^m}{dk^m} e^{-\frac{Dk^2}{2}t}}{\int_{-\infty}^{+\infty} dk e^{-Dk^2t}} \\ &= \frac{i^m \int_{-\infty}^{+\infty} dk e^{-Dk^2t} \left(\frac{Dt}{2}\right)^{\frac{m}{2}} H_m\left(\sqrt{\frac{Dt}{2}}k\right)}{\int_{-\infty}^{+\infty} dk e^{-Dk^2t}}, \end{aligned} \quad (\text{S22})$$

where $H_m\left(\sqrt{\frac{Dt}{2}}k\right)$ with $m = 0, 1, 2, \dots$ are the Hermite polynomials. In Eq. (S22), we have approximated $f_-(k)$ as a constant because k -dependent terms in $f_-(k)$ lead to higher-order terms of $1/\sqrt{Dt}$, which are negligible for large t . We have also extended the range of integration to $(-\infty, +\infty)$ since large- k terms have a low growth rate compared to terms with $k \simeq 0$ and thus are negligible. Utilizing Eq. (S22) and the generating function of the Hermite polynomials $\sum_{m=0}^{\infty} H_m(y) \frac{z^m}{m!} = \exp(2yz - z^2)$, we can obtain the moment generating function of x ,

$$\begin{aligned} \langle \exp[\xi x(t)] \rangle &\simeq \frac{\int_{-\infty}^{+\infty} dk \exp(-Dk^2t + \frac{Dt}{2}\xi^2 + i\xi Dtk)}{\int_{-\infty}^{+\infty} dk \exp(-Dk^2t)} \\ &= \exp\left[\frac{\xi^2}{2} \left(\sqrt{\frac{Dt}{2}}\right)^2\right]. \end{aligned} \quad (\text{S23})$$

The right-hand side of Eq. (S23) corresponds to the moment generating function of the Gaussian distribution, which means that dynamics exhibits asymptotically diffusive behavior with the standard deviation of x being $\sqrt{Dt}/2$ in the \mathcal{PT} -broken phase. The green broken line in Fig. S3 (c-2) shows $Dt/2$, which indicates that the analytical result agrees well with the numerical result.

S4. EVALUATION OF THE TRANSITION TIME FOR THE SHORT-TIME COMPLEXITY TRANSITION

We evaluate $t_{\text{dis}}^{\text{s/b}}$, which is the threshold time for the short-time dynamical complexity transition, through single-photon dynamics. Figure S4 shows numerically obtained transition times in both \mathcal{PT} -symmetric and \mathcal{PT} -broken phases, when two photons are initially put at $x_1^{\text{in}} = L/2$ with $\sigma_1^{\text{in}} = h$ and $x_2^{\text{in}} = L$ with $\sigma_2^{\text{in}} = v$. In the \mathcal{PT} -symmetric phase with $e^\gamma < e^{\gamma_{\mathcal{PT}}} \simeq 1.22$, $t_{\text{dis}}^{\text{s}}$ is proportional to the system size L . In unitary dynamics, it is known that the threshold time is proportional to the system size, which can be evaluated by the Lieb-Robinson bound [10]. In that sense, the behavior in the \mathcal{PT} -symmetric phase retains the structure found in unitary dynamics despite gain/loss terms. We also note that $t_{\text{dis}}^{\text{s}}$ is almost independent of γ and close to the threshold time for the unitary case, which can be seen from Fig. S4. In contrast, in the \mathcal{PT} -broken phase, single-photon

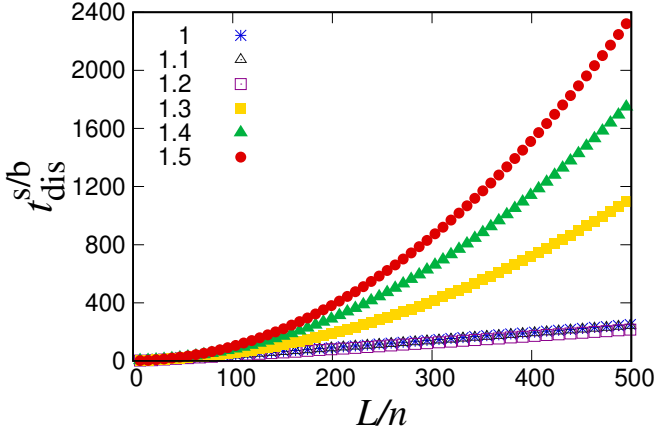


FIG. S4. System-size dependence of t_{dis}^s and t_{dis}^b with $\theta_1 = 0.65\pi$ and $\theta_2 = 0.25\pi$ when two photons $n = 2$ are initially located at $x_1^{\text{in}} = L/2$ with $\sigma_1^{\text{in}} = h$ and $x_2^{\text{in}} = L$ with $\sigma_2^{\text{in}} = v$. Each symbol corresponds to a different value of e^γ . The threshold time $t_{\text{dis}}^{s/b}$ in this figure is the smallest time at which $|P(t) - P_{\text{dis}}(t)| > \delta$ is satisfied with $\delta = 10^{-10}$. In the \mathcal{PT} -symmetric and \mathcal{PT} -broken phases, the transition times are linear and quadratic functions of the system size, respectively.

dynamics becomes diffusive as explained in the previous section. Then, t_{dis}^b is proportional to L^2 as shown in Fig. S4, which leads to $t_{\text{dis}}^b \gg t_{\text{dis}}^s$ in large systems.

To evaluate t_{dis}^b more quantitatively in the \mathcal{PT} -broken phase, we approximate the single-photon wave functions by Gaussian distributions on the basis of Eq. (S23). Also, we ignore the polarization $\sigma = h, v$ for simplicity. We consider a situation in which n photons are initially put at $x_p^{\text{in}} = \frac{L}{n}p$ with $p = 1, 2, \dots, n$, where Lp/n corresponds to In_p in the main text. In this case, the single-photon wave functions become

$$\psi_p(x, t) \propto \exp\left[-\frac{(x - \frac{L}{n}p)^2}{2Dt}\right]. \quad (\text{S24})$$

The matrix elements of $W(t)$ become $W_{pq}(t) = \psi_p(x_q^{\text{out}}, t)$. Here, x_q^{out} with $q = 1, 2, \dots, n$ is a position at which an output photon is detected, which corresponds to Out_q in the main text. While phases on $\psi_p(x_q^{\text{out}}, t)$ can take various values depending on x_q^{out} and t , we neglect effects of these phases. The ignorance of the phases is consistent with an inequality derived in Eq. (S33) below. Indeed, it means that we evaluate the L_1 -distance between distributions of photons and that of distinguishable particles larger than the actual value, not by taking cancellations of numerous terms with various phases into consideration. We write the difference between the actual photon distribution and the distribution of distinguishable particles as

$$P(\mathbf{y}) - P_{\text{dis}}(\mathbf{y}) \simeq \frac{\tilde{P}_{\text{dis}}(\mathbf{y}) + R(\mathbf{y})}{N(t)} - \frac{\tilde{P}_{\text{dis}}(\mathbf{y})}{N_{\text{dis}}(t)}, \quad (\text{S25})$$

where $\mathbf{y} = (x_1^{\text{out}}, x_2^{\text{out}}, \dots, x_n^{\text{out}}, t)$. Through Eq. (4) in the main text, we can understand that the terms in the numerator become

$$\tilde{P}_{\text{dis}}(\mathbf{y}) = \sum_{\omega} \prod_{p=1}^n |\psi_p(\mathbf{y}_{\omega[p]})|^2, \quad (\text{S26})$$

$$R(\mathbf{y}) = \sum_{\omega \neq \tau} \prod_{p=1}^n \psi_p(\mathbf{y}_{\omega[p]}) \psi_p^*(\mathbf{y}_{\tau[p]}), \quad (\text{S27})$$

where ω and τ in the sum are taken all over permutations, and $\mathbf{y}_q = (x_q^{\text{out}}, t)$. Here, we dropped $\prod_{j=1}^M n_j^{\text{out}}!$ assuming that probabilities where several photons are detected at the same position are negligibly small. In Eq. (S25), normalization factors $N(t)$ and $N_{\text{dis}}(t)$ become

$$N(t) = N_{\text{dis}}(t) + \sum_{\{x^{\text{out}}\}} R(\mathbf{y}), \quad (\text{S28})$$

$$N_{\text{dis}}(t) = \sum_{\{x^{\text{out}}\}} \tilde{P}_{\text{dis}}(\mathbf{y}). \quad (\text{S29})$$

Here, we assume $(L/n)^2 \gg Dt$ for analyzing the short-time complexity transition. For evaluating $R(\mathbf{y})$, we focus on a product of a specific pair $\psi_p(\mathbf{y}_{\omega[p]})$ and $\psi_{p'}^*(\mathbf{y}_{\tau[p']})$ in $R(\mathbf{y})$, where the permutations for p and p' coincide, i.e., $\omega(p) = \tau(p') = q$. Then, if we write $p' = p + \delta p$, we can evaluate $\psi_p(x_q^{\text{out}}, t) \psi_{p+\delta p}^*(x_q^{\text{out}}, t)$ as $\exp\left[-\frac{L^2(\delta p)^2}{4n^2 Dt}\right] |\tilde{\psi}_{p+\delta p/2}(x_q^{\text{out}})|^2$ with $\tilde{\psi}_{p+\delta p/2}(x)$ being the right-hand side of Eq. (S24), where $p + \delta p/2$ is substituted into p . Therefore, large δp leads to higher order terms of $\exp\left(-\frac{L^2}{4n^2 Dt}\right)$. Thus, due to the constraint $\omega \neq \tau$, leading terms of $R(\{\mathbf{y}\})$ become

$$R(\mathbf{y}) \simeq \sum_{\omega, p} \prod_{p_1=1}^{p-1} |\psi_{p_1}(\mathbf{y}_{\omega[p_1]})|^2 \prod_{p_2=p+2}^n |\psi_{p_2}(\mathbf{y}_{\omega[p_2]})|^2 \times 2\text{Re} [\Psi_p(\mathbf{y}_{\omega[p]}) \Psi_p^*(\mathbf{y}_{\omega[p+1]})], \quad (\text{S30})$$

where $\Psi_p(\mathbf{y}_{\omega[p]}) = \psi_p(\mathbf{y}_{\omega[p]}) \psi_{p+1}^*(\mathbf{y}_{\omega[p]})$. On the basis of Eq. (S30), we can evaluate the ratio of $N_{\text{dis}}(t)$ and $\sum_{\{x^{\text{out}}\}} R(\mathbf{y})$ as

$$\frac{\sum_{\{x^{\text{out}}\}} R(\mathbf{y})}{\sum_{\{x^{\text{out}}\}} \tilde{P}_{\text{dis}}(\mathbf{y})} \simeq 2n \exp\left(-\frac{L^2}{2n^2 Dt}\right). \quad (\text{S31})$$

Here, the factor n on the right-hand side originates from the number of cases where we choose a pair p and $p+1$. Thus, through the Taylor expansion of $1/N(t)$, the difference between the probability distribution of photons and that of the distinguishable particles becomes

$$P(\mathbf{y}) - P_{\text{dis}}(\mathbf{y}) \simeq \frac{R(\mathbf{y}) - \tilde{P}_{\text{dis}}(\mathbf{y}) 2ne^{-\frac{L^2}{2n^2 Dt}}}{N_{\text{dis}}(t)} \quad (\text{S32})$$

for $(L/n)^2 \gg Dt$. Equation (S32) results in an inequality

of the L_1 -distance between $P(\mathbf{y})$ and $P_{\text{dis}}(\mathbf{y})$,

$$\begin{aligned} |P(t) - P_{\text{dis}}(t)| &= \sum_{\{x_q^{\text{out}}\}} |P(\mathbf{y}) - P_{\text{dis}}(\mathbf{y})| \\ &\leq \sum_{\{x_q^{\text{out}}\}} \left| \frac{R(\mathbf{y})}{N_{\text{dis}}(t)} \right| + 2n \exp\left(-\frac{L^2}{2n^2 Dt}\right) \sum_{\{x_q^{\text{out}}\}} \left| \frac{\tilde{P}_{\text{dis}}(\mathbf{y})}{N_{\text{dis}}(t)} \right| \\ &\simeq 4n \exp\left(-\frac{L^2}{2n^2 Dt}\right). \end{aligned} \quad (\text{S33})$$

Therefore, the actual threshold time $t_{\text{dis}}^{\text{b}}$ at which $|P(t) - P_{\text{dis}}(t)| > \delta$ is satisfied for the first time is larger than the time at which $4n \exp(-L^2/2n^2 Dt) \simeq \delta$ is satisfied. This discussion leads to

$$t_{\text{dis}}^{\text{b}} > \frac{L^2}{2Dn^2 |\log(\delta/4n)|}. \quad (\text{S34})$$

The green broken line in Fig. S5 (a) represents the right-hand side of Eq. (S34) with $\delta = 10^{-10}$, which is below the numerically obtained $t_{\text{dis}}^{\text{b}}$, and thus verifies our inequality.

S5. EVALUATION OF THE TRANSITION TIME FOR THE LONG-TIME COMPLEXITY TRANSITION

We evaluate the threshold time t_{max} of the complexity transition for long-time dynamics by the gap size of the imaginary part of quasi-energies. Since the computability of $P(\{n^{\text{in}}\}, \{n^{\text{out}}\}, t)$ is based on the dominant eigenstate $|\phi_{\text{max}}^{\text{L/R}}\rangle$, the gap size $\Delta = |\varepsilon_{\text{max}} - \varepsilon_{\tilde{m}}|$ between $\varepsilon_{\text{max}} = i \log(\lambda_{\text{max}})$ and $\varepsilon_{\tilde{m}} = i \log(\lambda_{\tilde{m}})$ is important, where $|\lambda_{\text{max}}| = \max_l |\lambda_l| \equiv |\lambda_{l=l_{\text{max}}}|$ and $|\lambda_{\tilde{m}}| = \max_{l(\neq l_{\text{max}})} |\lambda_l|$. Note that $\lambda_{\tilde{m}}$ can be degenerate. Then, Δ^{-1} determines the timescale where the second dominant eigenstates $|\phi_{\tilde{m}}^{\text{L/R}}\rangle$ become negligible compared to the dominant state $|\phi_{\text{max}}^{\text{L/R}}\rangle$. In the present model, $\varepsilon_{\text{max}} = \varepsilon_-(k=0)$ and $\varepsilon_{\tilde{m}} = \varepsilon_-(k=\pm 2\pi/L)$, which results in

$$\Delta = \frac{D}{2} \left(\frac{2\pi}{L} \right)^2 \quad (\text{S35})$$

within the approximation in Eq. (S21). After long time evolution, $U^{\text{T}}(t) = V^t$ becomes

$$U^{\text{T}}(t) \simeq \lambda_{\text{max}}^t \left(|\phi_{\text{max}}^{\text{R}}\rangle \langle \phi_{\text{max}}^{\text{L}}| + e^{-\Delta t} \sum_{\tilde{m}} |\phi_{\tilde{m}}^{\text{R}}\rangle \langle \phi_{\tilde{m}}^{\text{L}}| \right) \quad (\text{S36})$$

where the sum for \tilde{m} includes two terms that correspond to $k = \pm 2\pi/L$ with $s = -$. We assume that dependence of $|\langle \text{Out}_q | \phi_{\tilde{m}}^{\text{R}} \rangle \langle \phi_{\tilde{m}}^{\text{L}} | \text{In}_p \rangle| / |\langle \text{Out}_q | \phi_{\text{max}}^{\text{R}} \rangle \langle \phi_{\text{max}}^{\text{L}} | \text{In}_p \rangle|$ on L is negligible for arbitrary p and q , compared to $e^{-\Delta t}$. Then, the matrix elements of $W(t)$, which determines

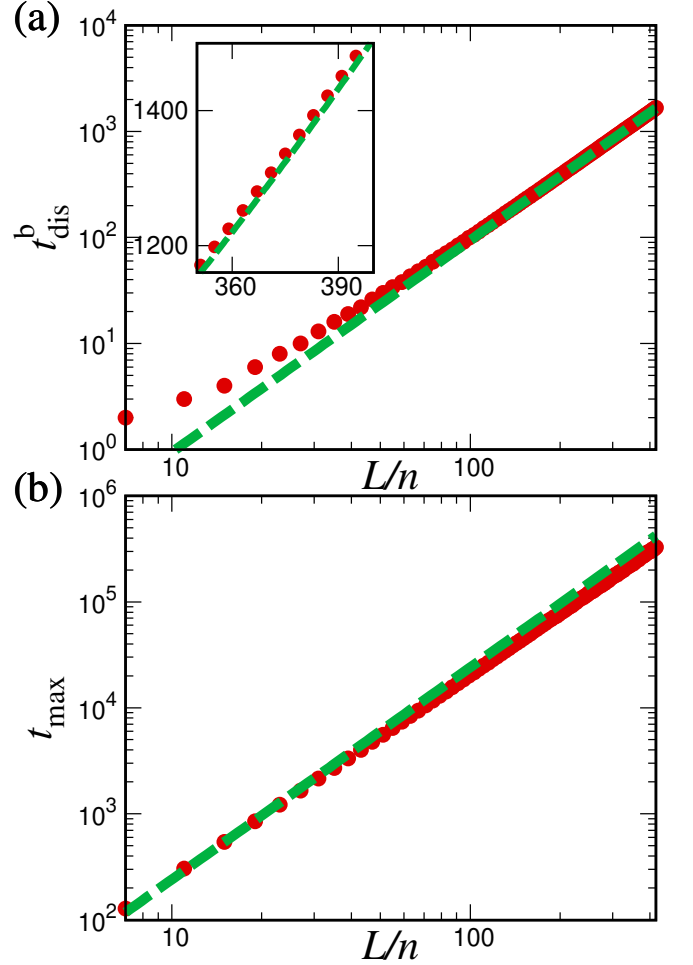


FIG. S5. System-size dependence of the threshold times at which dynamical complexity transitions occur in (a) short-time and (b) long-time scales when \mathcal{PT} symmetry is broken. In (a), red circles represent the numerically obtained smallest times at which $|P(t) - P_{\text{dis}}(t)| > \delta$ is satisfied. The green broken line shows $L^2/2Dn^2 |\log(\delta/4n)|$ in the right-hand side of Eq. (S34), which confirms the analytically derived inequality. In (b), red circles represent the threshold times for the long-time complexity transition at which $|P(t) - P_{\text{max}}| < \delta$ is satisfied for the first time in numerical simulations. The green broken line represents $L^2 |\log(\delta/8n)| / 2D\pi^2$ in the right hand side of Eq. (S41), which verifies the analytical result for sufficiently large L . In both (a) and (b), rotation angles are $\theta_1 = 0.65\pi$, $\theta_2 = 0.25\pi$, the gain-loss parameter is $e^\gamma = 1.5$, the number of photons is $n = 2$, the initial state is $\hat{b}_{x=L/2,h}^\dagger \hat{b}_{x=L,v}^\dagger |0\rangle$, and $\delta = 10^{-10}$.

the photon probability distribution, can be evaluated as

$$\begin{aligned} W_{pq}^*(t) &\simeq (\lambda_{\text{max}}^*)^t \langle \text{Out}_q | \phi_{\text{max}}^{\text{R}} \rangle \langle \phi_{\text{max}}^{\text{L}} | \text{In}_p \rangle \\ &\quad [1 + \sum_{\tilde{m}} R_q^{\tilde{m}} L_p^{\tilde{m}} e^{-\Delta t}], \end{aligned} \quad (\text{S37})$$

where $R_q^{\tilde{m}} = \langle \text{Out}_q | \phi_{\tilde{m}}^{\text{R}} \rangle / \langle \text{Out}_q | \phi_{\text{max}}^{\text{R}} \rangle$ and $L_p^{\tilde{m}} = \langle \phi_{\tilde{m}}^{\text{L}} | \text{In}_p \rangle / \langle \phi_{\text{max}}^{\text{L}} | \text{In}_p \rangle$. The permanent of $W^*(t)$ becomes

$$\text{Per}[W^*(t)] \simeq (\lambda_{\text{max}}^*)^{nt} \text{Per}[Z(t)] \prod_{p=1}^n \langle \text{Out}_p | \phi_{\text{max}}^{\text{R}} \rangle \langle \phi_{\text{max}}^{\text{L}} | \text{In}_p \rangle, \quad (\text{S38})$$

where $Z_{pq}(t) = [1 + \sum_{\tilde{m}} R_q^{\tilde{m}} L_p^{\tilde{m}} e^{-\Delta t}]$. Since $R_q^{\tilde{m}} L_p^{\tilde{m}}$ is a complex quantity, cancellations of numerous terms with various phases occur if we compute $|\text{Per}[Z(t)]|$. Then, $|\text{Per}[Z(t)]|$ is smaller than $n![1 + \mathcal{O}(2ne^{-\Delta t})]$. This discussion leads to the evaluation of the L_1 -distance between $P(\{n^{\text{in}}\}, \{n^{\text{out}}\}, t)$ and $P_{\text{max}}(\{n^{\text{out}}\})$ as

$$|P(t) - P_{\text{max}}| < \sum_{\{n^{\text{out}}\}} \frac{\prod_p |\langle \text{Out}_p | \phi_{\text{max}}^{\text{R}} \rangle|^2}{\prod_j n_j^{\text{out}}!} \left[\frac{1 + \mathcal{O}(4ne^{-\Delta t})}{\tilde{N}(t)} - \frac{1}{N_{\text{max}}} \right], \quad (\text{S39})$$

where $N_{\text{max}} = \sum_{\{n^{\text{out}}\}} \prod_p |\langle \text{Out}_p | \phi_{\text{max}}^{\text{R}} \rangle|^2 / \prod_j n_j^{\text{out}}!$ and $\tilde{N}(t) \simeq N_{\text{max}}[1 + \mathcal{O}(4ne^{-\Delta t})]$. Here, we put an assumption $|\langle \text{Out}_p | \phi_{\text{max}}^{\text{R}} \rangle| \simeq 1/\sqrt{M}$ for arbitrary p , which is valid in translational invariant systems. Then, through the Taylor expansion of $[1 + \mathcal{O}(4ne^{-\Delta t})]^{-1}$, the L_1 -norm of $P(\{n^{\text{in}}\}, \{n^{\text{out}}\}, t) - P_{\text{max}}(\{n^{\text{out}}\})$ can be evaluated as

$$|P(t) - P_{\text{max}}| < \mathcal{O}(8ne^{-\Delta t}). \quad (\text{S40})$$

Equation (S40) results in

$$t_{\text{max}} < -\frac{2L^2}{D(2\pi)^2} \log \left[\frac{\delta}{8n} \right], \quad (\text{S41})$$

where t_{max} is the time at which $|P(t) - P_{\text{max}}|$ becomes smaller than δ for the first time. Figure S5 (b) shows that the derived inequality is indeed satisfied.

S6. DYNAMICAL COMPLEXITY TRANSITION THROUGH REDUCTION OF MATRIX RANK

We can also analyze the long-time dynamical complexity transition from the viewpoint of matrix rank. It is known that we can compute $\text{Per}[W(t)]$ with

polynomial computational time $\mathcal{O}(n^{r-1})$ if the rank of the $n \times n$ matrix $W(t)$ is r [11]. In the \mathcal{PT} -broken phase, some eigenstates corresponding to large $|\lambda_l|$ become dominant as time evolves. If we sort eigenvalues of V as $|\lambda_1| \geq |\lambda_2| \geq \dots \geq |\lambda_M|$ and neglect lower order terms with $l < r$, we can approximate $U(t)$ as

$$U^{\text{T}}(t) \simeq \sum_{l=1}^r \lambda_l^t |\phi_l^{\text{R}}\rangle \langle \phi_l^{\text{L}}|. \quad (\text{S42})$$

In the right-hand side of Eq. (S42), the rank of each term in the sum is 1, which indicates that the rank of $U(t)$ is approximately smaller than or equal to r . This is because $\text{rank}(A+B) \leq \text{rank}(A) + \text{rank}(B)$ is satisfied for arbitrary matrices A and B . Thanks to a similar discussion, the rank of $W(t)$ is also smaller than or equal to r approximately.

Here, we put a cutoff $\tilde{\delta}$ and neglect components that satisfy $|\lambda_l/\lambda_1|^t < \tilde{\delta}$. In the present model, where the dispersion relation of the growing modes can be approximated as Eq. (S21), we can evaluate the ratio as $|\lambda_l/\lambda_1| = |\lambda_-(k)/\lambda_-(k=0)| \simeq \exp(-Dk^2/2)$, where $l = kL/\pi$ for $k > 0$ and $l = |kL/\pi| + 1$ for $k < 0$. When a momentum \tilde{k} satisfies

$$\exp\left(-\frac{D\tilde{k}^2}{2}t\right) \simeq \tilde{\delta}, \quad (\text{S43})$$

the number of eigenstates that satisfy $|\lambda_-(k)/\lambda_-(k=0)|^t > \tilde{\delta}$ becomes $2|\tilde{k}|/(2\pi/L)$, which corresponds to r . If the rank of $W(t)$ can be approximated by an n -independent value $r_c < n$, we can efficiently compute $\text{Per}[W(t)]$ with the algorithm in Ref. [11]. Here, we define a threshold time t_{rank} as the smallest time at which we can compute $P(\{n^{\text{in}}\}, \{n^{\text{out}}\}, t)$ by approximating the rank of $U(t)$ by r_c within the precision $\tilde{\delta}$. Then, we can evaluate t_{rank} as

$$t_{\text{rank}} \simeq \frac{2|\log(\tilde{\delta})|}{D\pi^2} \left(\frac{L}{r_c}\right)^2 \gg \frac{2|\log(\tilde{\delta})|}{D\pi^2} \left(\frac{L}{n}\right)^2. \quad (\text{S44})$$

While a more detailed evaluation of t_{rank} based on comparing $P(\{n^{\text{in}}\}, \{n^{\text{out}}\}, t)$ and the distribution obtained through the algorithm in [11] may result in corrections to the right-hand side of Eq. (S44), such as $\log(n)$ in Eq. (S41), we believe that such effects are negligible for sufficiently small $\tilde{\delta}$ and large L/n .

-
- [1] B. Do, M. L. Stohler, S. Balasubramanian, D. S. Elliott, C. Eash, E. Fischbach, M. A. Fischbach, A. Mills, and B. Zwickl, Experimental realization of a quantum quincunx by use of linear optical elements, *JOSA B* **22**, 499 (2005).
 [2] M. A. Broome, A. Fedrizzi, B. P. Lanyon, I. Kassal, A. Aspuru-Guzik, and A. G. White, Discrete single-

- photon quantum walks with tunable decoherence, *Phys. Rev. Lett.* **104**, 153602 (2010).
 [3] T. Kitagawa, M. A. Broome, A. Fedrizzi, M. S. Rudner, E. Berg, I. Kassal, A. Aspuru-Guzik, E. Demler, and A. G. White, Observation of topologically protected bound states in photonic quantum walks, *Nature communications* **3**, 882 (2012).

- [4] Y.-y. Zhao, N.-k. Yu, P. Kurzyński, G.-y. Xiang, C.-F. Li, and G.-C. Guo, Experimental realization of generalized qubit measurements based on quantum walks, *Phys. Rev. A* **91**, 042101 (2015).
- [5] F. Cardano, M. Maffei, F. Massa, B. Piccirillo, C. De Lisio, G. De Filippis, V. Cataudella, E. Santamato, and L. Marrucci, Statistical moments of quantum-walk dynamics reveal topological quantum transitions, *Nature communications* **7**, 11439 (2016).
- [6] X.-Y. Xu, Q.-Q. Wang, S.-J. Tao, W.-W. Pan, Z. Chen, M. Jan, Y.-T. Zhan, K. Sun, J.-S. Xu, Y.-J. Han, C.-F. Li, and G.-C. Guo, Experimental classification of quenched quantum walks by dynamical chern number, *Phys. Rev. Research* **1**, 033039 (2019).
- [7] L. Xiao, X. Zhan, Z. Bian, K. Wang, X. Zhang, X. Wang, J. Li, K. Mochizuki, D. Kim, N. Kawakami, W. Yi, H. Obuse, B. C. Sanders, and P. Xue, Observation of topological edge states in parity–time-symmetric quantum walks, *Nature Physics* **13**, 1117 (2017).
- [8] L. Xiao, T. Deng, K. Wang, G. Zhu, Z. Wang, W. Yi, and P. Xue, Non-Hermitian bulk–boundary correspondence in quantum dynamics, *Nature Physics* **16**, 761 (2020).
- [9] K. Mochizuki, D. Kim, and H. Obuse, Explicit definition of \mathcal{PT} symmetry for nonunitary quantum walks with gain and loss, *Phys. Rev. A* **93**, 062116 (2016).
- [10] A. Deshpande, B. Fefferman, M. C. Tran, M. Foss-Feig, and A. V. Gorshkov, Dynamical phase transitions in sampling complexity, *Phys. Rev. Lett.* **121**, 030501 (2018).
- [11] A. I. Barvinok, Two algorithmic results for the traveling salesman problem, *Mathematics of Operations Research* **21**, 65 (1996).